Cellular/Molecular

Changes in Presynaptic Gene Expression during Homeostatic Compensation at a Central Synapse

Evan R. Harrell, Diogo Pimentel, and Gero Miesenböck
Centre for Neural Circuits and Behaviour, University of Oxford, Oxford OX1 3SR, United Kingdom

Homeostatic matching of pre- and postsynaptic function has been observed in many species and neural structures, but whether transcriptional changes contribute to this form of trans-synaptic coordination remains unknown. To identify genes whose expression is altered in presynaptic neurons as a result of perturbing postsynaptic excitability, we applied a transcriptomics-friendly, temperature-inducible Kir2.1-based activity clamp at the first synaptic relay of the *Drosophila* olfactory system, a central synapse known to exhibit trans-synaptic homeostatic matching. Twelve hours after adult-onset suppression of activity in postsynaptic antennal lobe projection neurons of males and females, we detected changes in the expression of many genes in the third antennal segment, which houses the somata of presynaptic olfactory receptor neurons. These changes affected genes with roles in synaptic vesicle release and synaptic remodeling, including several implicated in homeostatic plasticity at the neuromuscular junction. At 48 h and beyond, the transcriptional landscape tilted toward protein synthesis, folding, and degradation; energy metabolism; and cellular stress defenses, indicating that the system had been pushed to its homeostatic limits. Our analysis suggests that similar homeostatic machinery operates at peripheral and central synapses and identifies many of its components. The presynaptic transcriptional response to genetically targeted postsynaptic perturbations could be exploited for the construction of novel connectivity tracing tools.

Key words: **gene expression; homeostatic plasticity; synaptic reorganization; synaptic transmission; trans-synaptic signaling; transcriptomics**

Significance Statement

Homeostatic feedback mechanisms adjust intrinsic and synaptic properties of neurons to keep their average activity levels constant. We show that, at a central synapse in the fruit fly brain, these mechanisms include changes in presynaptic gene expression that are instructed by an abrupt loss of postsynaptic excitability. The trans-synaptically regulated genes have roles in synaptic vesicle release and synapse remodeling; protein synthesis, folding, and degradation; and energy metabolism. Our study establishes a role for transcriptional changes in homeostatic synaptic plasticity, points to mechanistic commonalities between peripheral and central synapses, and potentially opens new opportunities for the development of connectivity-based gene expression systems.

Received Nov. 25, 2020; revised Jan. 27, 2021; accepted Jan. 28, 2021.

Author contributions: E.R.H. and G.M. designed research; E.R.H. and D.P. performed research; E.R.H. and G.M. contributed unpublished reagents/analytic tools; E.R.H., D.P., and G.M. analyzed data; E.R.H. and G.M. wrote the paper.

E.R. Harrell's present address: Institute Pasteur, Institut National de la Santé et de la Recherche Médicale, Hearing Institute, 63 rue de Charenton, F-75012 Paris, France.

This work was supported by Wellcome grants 209235/Z/17/Z, 106988/Z/15/Z, 090309/Z/09/Z, and 089270/Z/09/Z; Gatsby Charitable Foundation grant GAT3237; and European Research Council grant 832467. We thank Paul Overton for providing advice on RNA isolation; Amélie Baud for giving many helpful tips for the gene ontology analysis; Ruth Brain for assisting with stock maintenance and dissections; Jessica Beevers for helping with dissections and making delicious fly food (from the flies' perspective); and Ronald Davis, Jeffrey Hall, Mani Ramaswami, Gerald Rubin, and Reinhard Stocker for kindly sharing reagents.

The authors declare no competing financial interests.

Correspondence should be addressed to at Evan R. Harrell at evan-richard.harrell@pasteur.fr or Gero Miesenböck at gero.miesenboeck@cncb.ox.ac.uk.

https://doi.org/10.1523/JNEUROSCI.2979-20.2021

Introduction

Homeostatic feedback that stabilizes network activity after synaptic weight changes is an important adjunct to correlation-based learning rules (Turrigiano, 2011). Early demonstrations of homeostatic plasticity followed pharmacological manipulations of synaptic transmission in neuronal cultures (Turrigiano et al., 1994, 1998). When global activity levels were artificially increased or decreased, homeostatic forces intervened to maintain firing rates within defined ranges. These homeostatic forces are generated by two processes (Turrigiano, 2011): cell-autonomous changes in intrinsic excitability, which alter the gain of the neuronal voltage response to synaptic currents (Turrigiano et al., 1994; Desai et al., 1999); and adjustments of the synaptic strengths themselves (Petersen et al., 1997; Davis et al., 1998; Turrigiano et al., 1998; Burrone et al., 2002). These adjustments, though in principle achievable in cell-autonomous fashion by altering

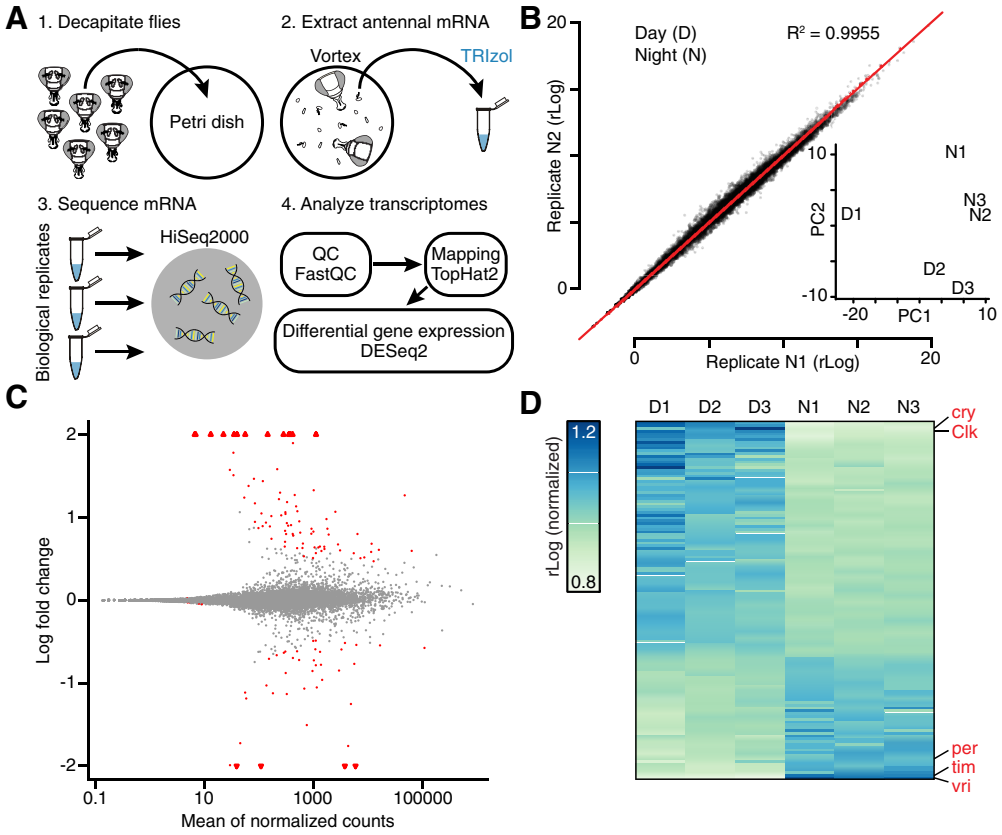

Figure 1. Antennal transcriptomics: workflow, diagnostics, and functional validation. ***A***, Experimental workflow. ***B***, Scatterplot of gene expression levels in biological replicates N1 versus N2. Inset, D and N samples in a principal component analysis (PCA) plot. ***C***, MA plot of $\log_2$ fold change in expression (M) versus mean expression level (A) of all transcripts. Triangles represent data points outside the plotted range. ***D***, Expression levels of all transcripts with FDR-adjusted $p < 0.20$ during the day and night. Each column represents a sequencing library generated from third antennal segments. Red type indicates core clock components.

the density of neurotransmitter receptors in the postsynaptic membrane (Wierenga et al., 2005; Goold and Nicoll, 2010), often involve a trans-synaptic partnership in which postsynaptic neurons communicate deviations from their activity setpoint via retrograde signals to their presynaptic partners, which in turn increase or decrease transmitter release (Cull-Candy et al., 1980; Petersen et al., 1997; Sandrock et al., 1997; Davis et al., 1998; Burrone et al., 2002; Haghighi et al., 2003; Thiagarajan et al., 2005).

Much existing knowledge of retrograde homeostatic communication comes from studies of the neuromuscular junction (NMJ). In mammals and *Drosophila*, mutations or autoantibodies that reduce the responsiveness of muscle to neurotransmitter cause compensatory increases in motor neuron vesicular release (Cull-Candy et al., 1980; Petersen et al., 1997; Sandrock et al., 1997; Davis et al., 1998). At the *Drosophila* NMJ, acute pharmacological receptor blockade (Frank et al., 2006) or expression of the inwardly rectifying potassium channel Kir2.1 in muscle (Paradis et al., 2001) induces similar presynaptic compensatory effects. While many gene products and signaling pathways have been implicated in synaptic homeostasis (Davis and Müller, 2015), knowledge of the transcriptional changes that may be required to lock the presynaptic cells into their altered functional state remains scant (Marie et al., 2010).

Pre- and postsynaptic function are also matched at the central synapses between olfactory receptor neurons (ORNs) and projection neurons (PNs) in the antennal lobe of *Drosophila* (Kazama and Wilson, 2008), where the axons of 20-200 ORNs expressing the same odorant receptor connect to dendrites of an average of three affine PNs in a precise anatomic register (Groschner and Miesenböck, 2019). There is clear covariation between the dendritic arbor sizes of PNs belonging to different transmission channels and the amplitudes of unitary EPSCs: the larger unitary EPSCs of PNs with larger dendritic trees (and, therefore, lower impedances) reflect homeostatic increases in the number of presynaptic ORN release sites in response to increased postsynaptic demand for synaptic drive (Kazama and Wilson, 2008; Mosca and Luo, 2014). This central model of synaptic homeostasis has been characterized physiologically and anatomically, but the molecular mechanism of synaptic matching is unexplored. Taking advantage of the ease with which the presynaptic partners at this synapse can be isolated (they reside in an external appendage, the third antennal segment), we conducted a transcriptome-wide screen for genes regulated by retrograde homeostatic signals. Homeostatic plasticity was induced by adult-onset expression of Kir2.1 in PNs; the expression of a nonconducting mutant of Kir2.1 (Kir2.1-nc) served as control.

Materials and Methods

Drosophila *strains and culture.* Flies were maintained at 21°C and 65% humidity on a constant 12:12 h light:dark cycle in rich cornmeal and molasses-based food with brewer's yeast. Driver lines *GH146-GAL4* (Stocker et al., 1997) and *pdf-GAL4* (Renn et al., 1999) were used to target the expression of codon-optimized *UAS-Kir2.1* transgenes (see below) to PNs and PDF-expressing clock neurons, respectively. Three copies of two *tubulin-GAL80^{ts}* insertions on different chromosomes (McGuire et al., 2003) were combined to achieve tight repression of the

Table 1. Mapping metrics of third antennal segment transcriptomes collected during the day (D) and night (N)[a]

ID	*n* Reads	*n* Mapped	% Mapped	*n* Unique	% Unique	Average R^2
D1	20,857,542	14,732,179	70.63	13,342,850	63.97	0.9897
D2	19,466,527	14,408,098	74.01	13,373,355	68.70	0.9931
D3	18,908,595	14,656,324	77.51	13,440,037	71.08	0.9919
N1	22,905,480	18,406,329	80.36	17,187,773	75.04	0.9955
N2	21,095,058	16,864,414	79.94	15,564,220	73.78	0.9963
N3	23,547,296	18,429,070	78.26	16,918,247	71.85	0.9963
Average	21,130,083	16,249,402	76.79	14,971,080	70.74	0.9938

[a]Absolute numbers and percentages of reads aligned to Ensembl DM genome release 5.74. *n* Reads, number of raw reads; *n* Mapped and % Mapped, number of reads mapping to the reference genome with corresponding percentage; *n* Unique and % Unique, number of reads mapping to a unique location in the reference genome with corresponding percentage; Average R^2, average replicate correlation (Pearson's correlation coefficient calculated across all genes with a non-zero read count in at least one replicate).

GAL4-responsive transgenes until induction. The induction incubator was kept at 31°C in 70% humidity on the same 12:12 light:dark schedule.

The cDNA sequence encoding human Kir2.1 was codon-optimized for *Drosophila* (GenBank accession number MW088713), synthesized at MWG Eurofins, and fused to a codon-optimized N-terminal EGFP tag. The nonconducting variant (Kir2.1-nc) was created by mutating codon 146 of the ion channel sequence from glycine to serine (GGA to AGC) (Haruna et al., 2007). The channel constructs replaced the *mCD8::GFP* coding sequence in derivatives of plasmid *pJFRC2-10XUAS-IVS-mCD8::GFP* (Pfeiffer et al., 2010), which were inserted into the *attp2* landing site on the third autosome.

Confocal microscopy. Female flies 5 d of age were anesthetized on ice and dissected in PBS (1.86 mM NaH_2PO_4, 8.41 mM Na_2HPO_4, 175 mM NaCl). Immediately after dissection, brains were fixed in ice-cold PBS containing 4% (w/v) PFA for 1-2 h at room temperature, rinsed 3 times in ice-cold PBS containing 0.1% (w/v) Triton X-100 (PBT), washed 3 times for 20 min in ice-cold PBT, and mounted and cleared in Vectashield (Vector Labs). Confocal image stacks with an axial spacing of 1-1.5 μm were collected on a Leica Microsystems TCS SP5 microscope with an HCX IRAPO L 25×0.95 W objective.

Electrophysiology. Targeted whole-cell patch-clamp recordings from the fluorescent somata of PNs expressing EGFP::Kir2.1 or EGFP::Kir2.1-nc were obtained through a small cranial window in 5-day-old females. The brain was continuously superfused with extracellular solution containing 103 mM NaCl, 3 mM KCl, 5 mM TES, 8 mM trehalose, 10 mM glucose, 7 mM sucrose, 26 mM $NaHCO_3$, 1 mM NaH_2PO_4, 1.5 mM $CaCl_2$, 4 mM $MgCl_2$, pH 7.3, and equilibrated with 95% O_2–5% CO_2. Borosilicate glass electrodes (7-13 MΩ) were filled with intracellular solution containing 140 mM potassium aspartate, 10 mM HEPES, 1 mM KCl, 4 mM Mg-ATP, 0.5 mM Na_3GTP, 1 mM EGTA, pH 7.3. Signals were acquired with a MultiClamp 700B Microelectrode Amplifier, filtered at 6-10 kHz, and digitized at 10-20 kHz with an ITC-18 data acquisition board controlled by the Nclamp and NeuroMatic packages. Data were analyzed with NeuroMatic (http://neuromatic.thinkrandom.com) and custom procedures in Igor Pro (WaveMetrics) (Donlea et al., 2014). The membrane time constant was determined by fitting a single exponential to the voltage deflection caused by a 200-ms-long hyperpolarizing current pulse. Input resistances were estimated from linear fits of the subthreshold voltage deflections elicited by 5 pA current pulses of increasing amplitude and a duration of 1 s. Firing rates were quantified by holding cells at resting potentials of –60 ± 2 mV and injecting sequences of depolarizing current pulses (5 pA increments, 1 s duration). Spikes were detected by finding minima in the second derivative of the membrane potential record. The spike rate was calculated by dividing the number of action potentials discharged by the time elapsed between the first and last spike. The current amplitude at which each cell reached a given frequency threshold (1-50 Hz) was used to construct cumulative distribution functions. The distributions were fit with logistic Naka-Rushton functions of the following form (Donlea et al., 2014):

Table 2. Circadian-regulated genes (FDR-adjusted $p < 0.01$)[a]

Gene	Baseline expression	Log_2 fold change	*p*	FDR	Description
vri	3724.50	−4.6985	4.29E-106	3.89E-102	core circadian clock[b]
tim	5834.10	−3.7979	4.29E-78	1.95E-74	core circadian clock[b]
GstD3	1104.77	2.5973	3.46E-28	1.05E-24	glutathione metabolism[b]
CG2016	281.15	2.9593	1.22E-22	2.77E-19	hormone binding
CG33757	410.74	2.9298	1.03E-19	1.87E-16	no functional information
Cyp4d21	4279.26	−1.8094	7.21E-18	1.09E-14	oxidation-reduction process[b]
Clk	143.92	2.9383	2.18E-16	2.82E-13	core circadian clock[b]
CG10026	352.82	2.3039	3.80E-15	4.31E-12	lipid binding
Ugt35b	46348.94	1.3358	3.54E-11	3.56E-08	UDP glycosyl transferase[b]
GstE9	1001.76	1.4003	2.71E-10	2.46E-07	glutathione metabolism[b]
CG31324	749.19	−1.6055	4.71E-09	3.88E-06	no functional information
Pdh	55.97	2.9461	7.75E-09	5.85E-06	receptor dehydrogenase[b]
CG6834	2496.64	1.1409	1.30E-08	9.04E-06	no functional information
CG7208	108.72	−2.2001	1.99E-08	1.29E-05	no functional information
mt:lrRNA	418.18	2.0580	1.64E-07	9.93E-05	mitochondrial translation
CG15096	1139.97	−1.1414	2.08E-07	1.14E-04	transmembrane anion transport
slik	449.97	1.3790	2.14E-07	1.14E-04	cell proliferation
CG9815	39.03	−3.1059	2.43E-07	1.23E-04	no functional information
cu	674.29	−1.1606	3.45E-07	1.57E-04	NADP metabolism[b]
zormin	503.40	1.1680	3.29E-07	1.57E-04	cytoskeletal structure
CG10513	326.16	1.2906	3.72E-07	1.61E-04	no functional information
Ugt86De	477.43	1.2370	5.25E-07	2.17E-04	UDP glycosyl transferase[b]
CG6484	322.18	−1.2398	7.35E-07	2.90E-04	glucose import
CheB93b	215.37	1.7419	1.21E-06	4.56E-04	pheromone detection
CG7149	1784.54	0.9488	1.49E-06	5.42E-04	phosphotransferase
CG31100	1430.28	−1.0624	2.34E-06	8.16E-04	glucose import
CG10433	1716.02	1.0842	2.70E-06	9.06E-04	female receptivity to mating
CG2930	545.58	1.0604	4.77E-06	1.55E-03	transmembrane transport
CG6356	4808.16	−1.4003	5.51E-06	1.72E-03	transmembrane transport
CG33946	117.51	1.6102	5.89E-06	1.78E-03	no functional information
wbl	231.65	1.3672	6.67E-06	1.95E-03	protein folding in ER
CG3625	6333.94	0.8930	7.49E-06	2.12E-03	no functional information
CG31321	34.98	2.6316	8.08E-06	2.22E-03	transmembrane transport
CG13841	243.03	1.4691	1.28E-05	3.42E-03	no functional information
CG7724	912.70	0.9733	1.44E-05	3.74E-03	oxidation-reduction process
Ugt35a	303.93	1.2040	1.63E-05	4.10E-03	UDP glycosyl transferase[b]
CG1698	22.34	3.7173	1.72E-05	4.22E-03	neurotransmitter transport
CG11951	39.60	2.5616	1.79E-05	4.26E-03	proteolysis
mt:ND2	385.70	1.0282	1.84E-05	4.29E-03	mitochondrial electron transport
CG6910	255.13	1.1671	2.27E-05	5.16E-03	oxidation-reduction process
cwo	1095.79	−0.8935	2.82E-05	6.24E-03	circadian regulation of gene expression[b]

[a]*p*, Unadjusted *p* value; FDR, *p* value adjusted for multiple comparisons.
[b]Known clock-controlled genes (Claridge-Chang et al., 2001; McDonald and Rosbash, 2001) or genes annotated as circadian-related in FlyBase.

$$F = F_{max}\frac{I^n}{I^n + I_{50}^n}$$

where F is the percentage of cells reaching threshold at a given current level I, F_{max} is the percentage of cells reaching threshold at maximal current, I_{50} indicates the half-maximal or semisaturation current, and the exponent n determines the steepness of the curve. With only two free parameters (I_{50} and n, given that F_{max} is measured experimentally), this simple model provided a satisfying fit to all distributions.

Circadian behavior. Three-day-old female flies were individually inserted into 65 mm glass tubes and loaded into the Trikinetics *Drosophila* Activity Monitoring system, which was operated at 31°C in 24 h dark conditions for 5–7 d. Group sizes for activity measurements (16 experimental and 16 control flies) reflect the capacity of the monitors.

Third antennal segment dissection. Groups of 20-30 flies were aged in precisely controlled temperature conditions for 5 d (see Fig. 4*A*) and decapitated with a surgical scalpel on a CO_2 pad; the heads were

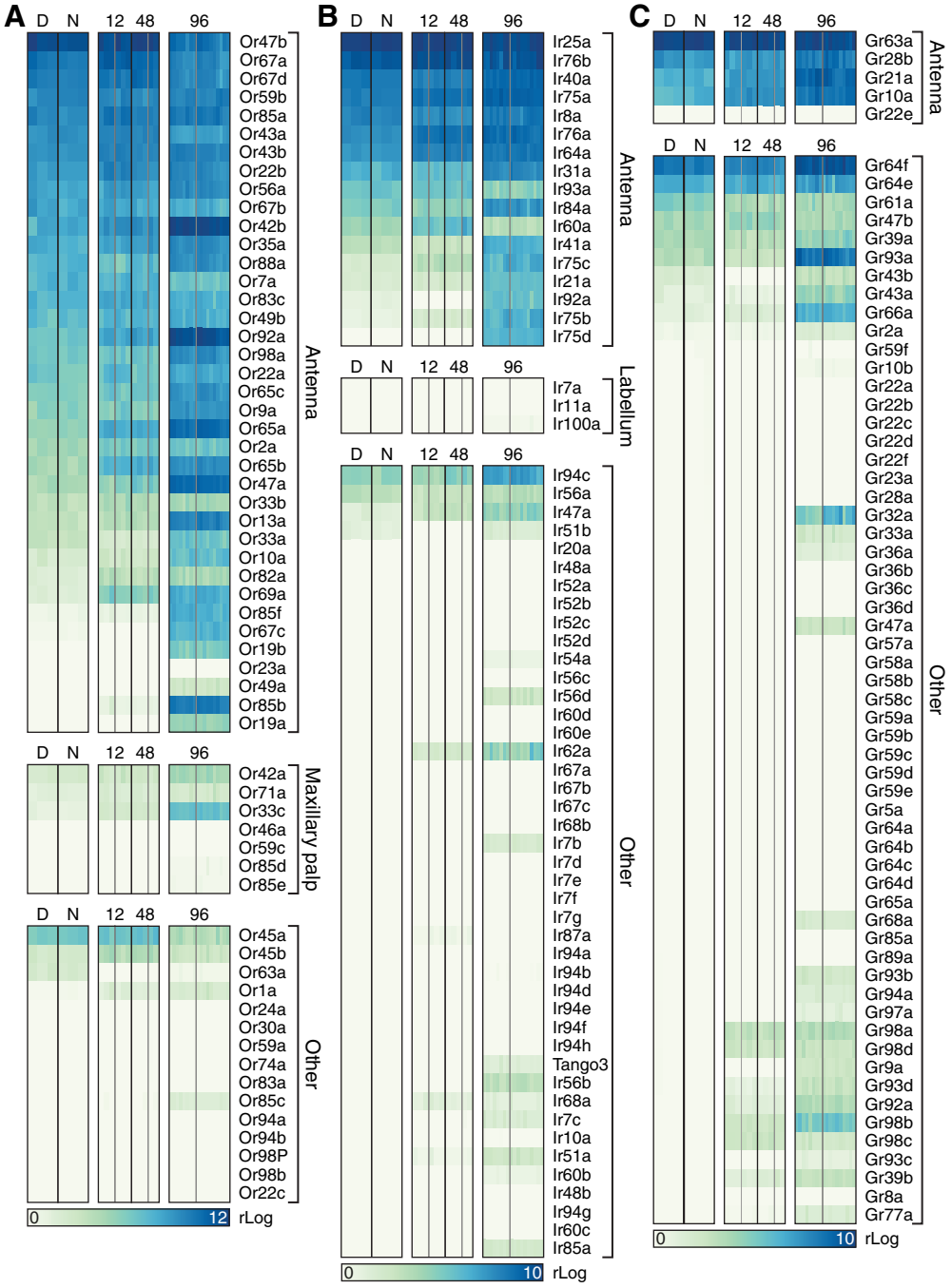

Figure 2. Expression levels of ORs (***A***), IRs (***B***), and GRs (***C***) in sequencing libraries generated from third antennal segments. Each column represents a library generated during the day (D) or night (N), or after 12, 48, or 96 h induction of Kir2.1 or Kir2.1-nc. Within each induction period, gray dividers separate libraries obtained from flies expressing Kir2.1 (to the left of the divider) from those of flies expressing Kir2.1-nc (to the right of the divider). The gene encoding the obligatory OR coreceptor Orco/Or83b was expressed at a level above those of other *OR* genes (mean rLog ± SEM = 13.6178 ± 0.16503) and omitted from ***A***.

transferred to Petri dishes kept on dry ice. Once a Petri dish contained ~50 heads, it was sealed with Parafilm and stored at −80°C until RNA extraction. The sealed Petri dishes were dipped in liquid nitrogen for 60 s, vortexed at full strength for 60 s, and then unsealed and placed on a dry-ice-chilled glass stand under a dissection microscope. Individual third antennal segments were picked with fine forceps and placed directly into 100 µl TRIzol (Thermo Fisher Scientific).

RNA extraction. Third antennal segments in 100 µl TRIzol were disrupted with several strokes in a Dounce homogenizer. The homogenates were diluted with 900 µl TRIzol and incubated at room temperature for 5 min. Samples destined for 3′ digital gene expression profiling (3′ DGE) underwent phase separation after the addition of 225 µl chloroform; RNA in the aqueous phase was precipitated with isopropanol and resuspended in 5 µl RNase-free water. Total RNA for RNA-seq and qRT-PCR was isolated with the help of RNeasy minelute columns (QIAGEN), following the addition of 400 µl of 70% RNase-free ethanol to the TRIzol homogenates and on-column DNaseI digests. Samples were snap frozen in liquid nitrogen and stored at −80°C.

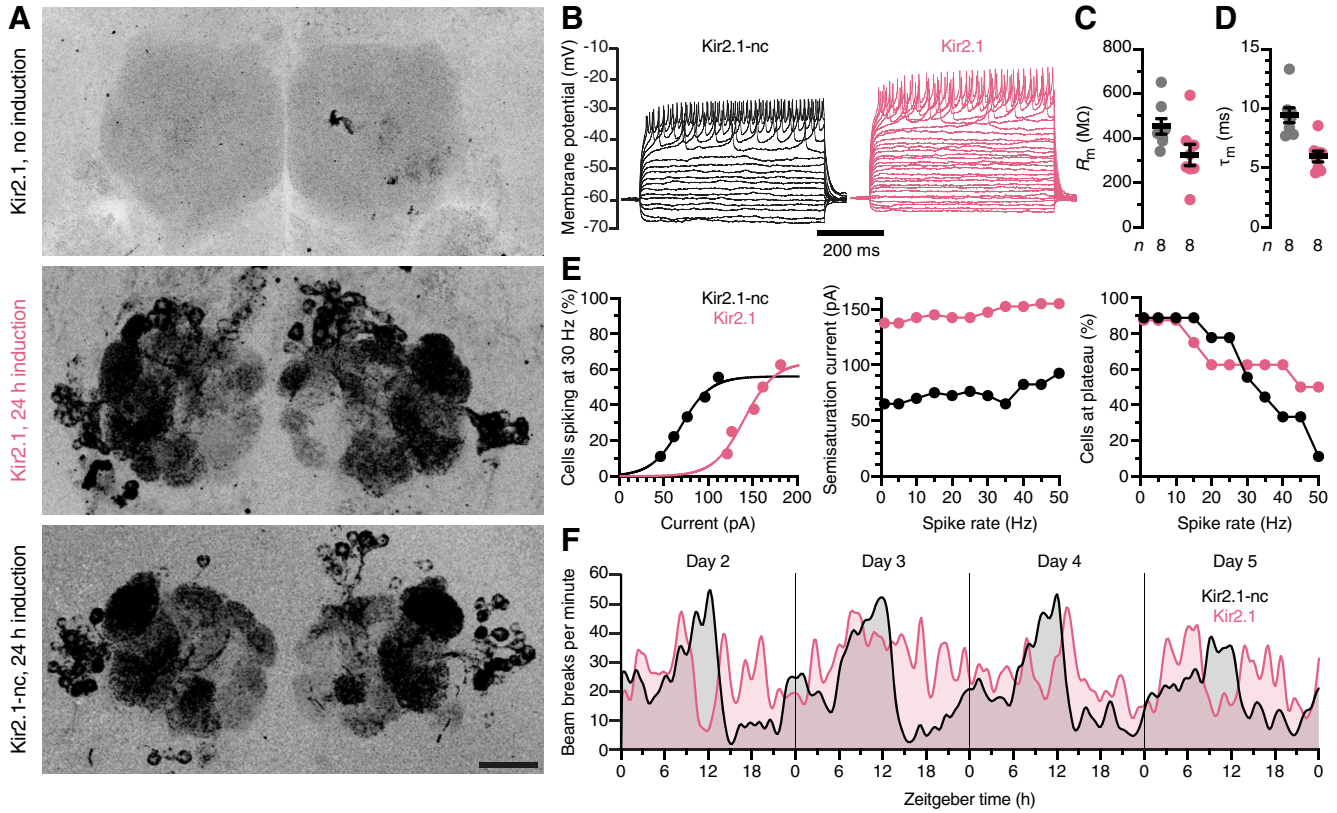

Figure 3. A transcriptomics-friendly neuronal activity clamp. ***A***, Maximum intensity projections of confocal image stacks through the antennal lobes of 5-day-old female flies carrying *EGFP::Kir2.1* or *EGFP::Kir2.1-nc* transgenes under *GH146-GAL4* and *tub-GAL80^{ts}* control. The expression of Kir2.1 constructs is undetectable at 21°C (top) but induced at 31°C (center and bottom). Scale bar, 20 µm. ***B***, Example voltage responses to 5 pA current steps of antennal lobe PNs expressing EGFP::Kir2.1-nc (black) or EGFP::Kir2.1 (red). ***C***, ***D***, Kir2.1 (red) lowers the input resistance R_m ($t_{(14)} = 2.1652$, $p = 0.0481$; ***C***) and shortens the membrane time constant τ_m ($t_{(14)} = 4.4959$, $p = 0.0005$; ***D***) relative to Kir2.1-nc (black). Circles represent individual PNs. Error bars indicate mean ± SEM. ***E***, Cumulative distribution functions of the percentages of PNs reaching a spike frequency of 30 Hz at different levels of injected current (left); semisaturation currents (middle) and percentages of cells reaching spike rates of 1-50 Hz, for PNs expressing Kir2.1-nc (black) or Kir2.1 (red). ***F***, Circadian locomotor rhythms in constant darkness. Locomotion was quantified as the total number of midline crossings per minute in groups of 16 flies expressing Kir2.1-nc (black) or Kir2.1 (red) under *pdf-GAL4* control. The traces were smoothed with a Gaussian kernel (1.25 h FWHM) and show data collected on days 2-5 after the flies were transferred to activity monitors.

cDNA library generation. Libraries for 3′ DGE were generated at MWG Eurofins Genomics from ultrasonically fragmented poly(A)-tailed RNA, which was isolated using oligo(dT) chromatography. Following ligation of an RNA adapter to the 5'-end, the mRNA fragments were reverse-transcribed from an oligo(dT) primer, and the resulting cDNA was PCR-amplified with a high-fidelity polymerase. Each cDNA library was purified, size-selected, quality-checked by capillary electrophoresis, and sequenced on the HiSeq2000 platform (Illumina) in 1 × 100 bp run mode.

For RNA-seq and qRT-PCR, oligo(dT)-enriched RNA underwent 14 cycles of amplification using the SMARTer Ultra Low RNA Kit for Illumina Sequencing (Clontech). After cDNA fragmentation, libraries were prepared in an additional 15 amplification cycles using the NEBNext Ultra DNA Library Prep Kit for Illumina (New England Biolabs) and sequenced on the HiSeq2000 platform (Illumina) in paired-end mode.

Transcriptome analysis. Raw reads were 100 bp in length (paired-end reads for RNA-seq and single-ended reads for 3′ DGE). Fastq files, containing reads and quality scores, were first run through the FastQC package (Andrews, 2010). Highly abundant sequences that did not map to the *Drosophila* genome (and originated from primers or amplification artifacts) were eliminated using Trimmomatic software (Bolger et al., 2014). Reads were scanned with a 4 bp sliding window and cut when the average quality dropped to <15; trimmed reads <25 bp were discarded. The reads were mapped to Ensembl DM genome release 5.74 using TopHat2 (D. Kim et al., 2013), assigned to transcripts annotated in the transcript file of the Berkeley Drosophila Genome Project release 5.74 with Cufflinks, and merged into an experiment-wide gtf file with Cuffmerge (Trapnell et al., 2012). The gtf file was used to produce raw read counts (using HTSeq) suitable for differential expression analysis in DESeq2 (Love et al., 2014). The topGO and *ViSEAGO* packages were used to analyze the enrichment of gene ontology (GO) terms in the set of differentially expressed genes called by DESeq2 (unadjusted $p < 0.05$) vis-à-vis a reference set of all genes with a normalized expression level above 1 (the "gene universe") (Alexa et al., 2006; Brionne et al., 2019). To keep the number of Fisher's exact tests to a minimum, only GO terms with >40 attached genes were considered. Enriched GO terms with unadjusted $p < 0.01$ were clustered hierarchically according to Wang's distance, a measure of semantic similarity (J. Z. Wang et al., 2007; Brionne et al., 2019).

qRT-PCR. Transcript levels were determined by qRT-PCR on a LightCycler 480 system (Roche Diagnostics) using SYBR Green I Master Mix (Roche Diagnostics) in 10 µl reactions containing 100 nM of each gene-specific primer and 50 ng of preamplified cDNA. Two sets of primers were designed for each gene of interest. All samples were run in technical triplicates; non–reverse-transcribed mRNA and water served as negative controls. Melting curves were analyzed after amplification, and amplicons were visualized by agarose gel electrophoresis to confirm primer specificity. Relative transcript levels were estimated with the help of the $2^{-\Delta\Delta Ct}$ method (Livak and Schmittgen, 2001), using the housekeeping gene *CycK* for normalization.

Experimental design and statistical analysis. Sample sizes for differential gene expression analyses were determined in a pilot experiment comparing the expression of circadian-regulated genes during the day and night (Fig. 1*D*). No statistical tests were used to predetermine sample sizes for electrophysiology, behavior, or qRT-PCR.

Statistical analyses of differential gene expression data and GO term enrichment relied on built-in functions in DESeq2, topGO, and *ViSEAGO*, as described above (Alexa et al., 2006; Love et al., 2014;

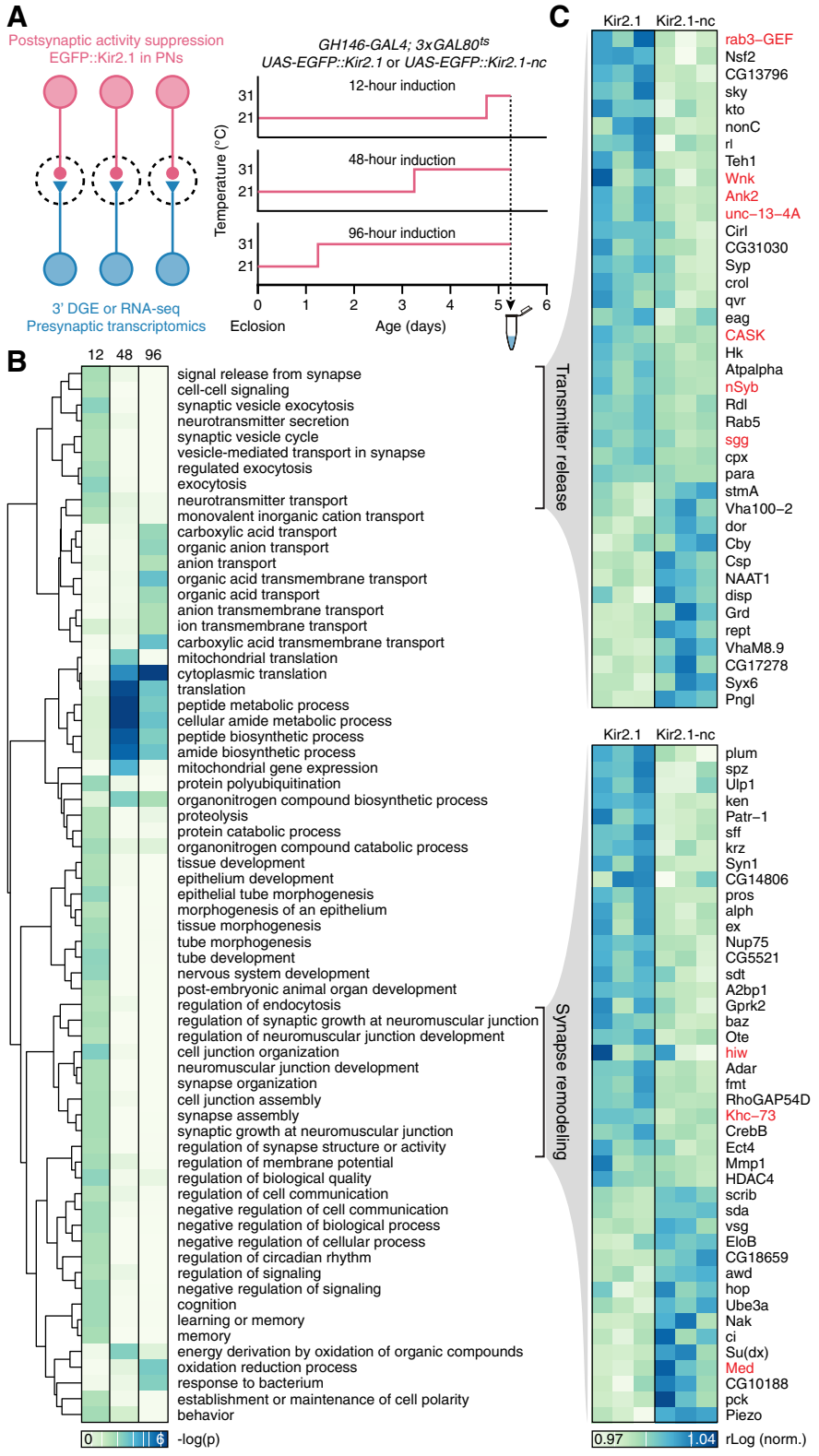

Figure 4. Trans-synaptic regulation of gene expression: transmitter release and synapse remodeling, and a late shift to proteostasis and neuroprotection. ***A***, Experimental design. ***B***, Enrichment of GO biological process terms in third antennal segment transcriptomes after 12, 48, and 96 h induction of Kir2.1. The dendrogram represents semantic groupings among GO terms. ***C***, Expression levels of transcripts attached to two semantic groupings, "transmitter release" and "synapse remodeling" (***B***), after 12 h of induction of Kir2.1 or Kir2.1-nc. Each column represents a sequencing library. Red type indicates gene products previously implicated in homeostatic synaptic plasticity (see Discussion).

Brionne et al., 2019). Hypotheses about differentially expressed genes were evaluated by Wald test in DESeq2 (Love et al., 2014); enrichment of GO terms was quantified using Fisher's exact test in *ViSEAGO* (Brionne et al., 2019). Group means of electrophysiological parameters, which Shapiro–Wilk tests confirmed were normally distributed, were compared by two-tailed *t* test.

Transcriptome data are available from the European Bioinformatics Institute's ArrayExpress archive under accession numbers E-MTAB-10 062 (antennal gene expression during the day and night) and E-MTAB-10 065 (antennal gene expression following the induction of Kir2.1 or Kir2.1-nc in PNs).

Results

Antennal transcriptomics

To characterize gene expression in the third antennal segment, 5-day-old male Canton-S flies were decapitated either between zeitgeber time 5 (ZT5) and ZT8 (the day group) or between ZT17 and ZT20 (the night group). After snap-freezing, third antennal segments were manually isolated, and total RNA was extracted in a single batch to minimize variability (Fig. 1*A*; see Materials and Methods). For both day and night conditions, three biological replicates were prepared, and the resulting six cDNA libraries were sequenced on one lane of an Illumina HiSeq2000 machine using 3′ DGE technology. After stringent quality assessment and read trimming (Fig. 1*A*), the high-quality reads were mapped to the *Drosophila* genome (for mapping statistics, see Table 1). Biological replicates showed high correlations with one another (Fig. 1*B*; Table 1), and day and night samples could easily be distinguished on the basis of their top two principal components (Fig. 1*B*, inset). Underlying this clean separability were 128 differentially expressed genes, identified by DESeq2 (Love et al., 2014) with a false discovery rate (FDR)-adjusted significance level of < 0.20, and large expression level differences between the day and night (Fig. 1*C*; Table 2). Core clock components, such as cryptochrome, Clock, period, timeless, and vrille, were found near the top of the amplitude distribution of oscillating transcripts, in two groups at opposite poles of the 24 h cycle (Fig. 1*C*), consistent with their antagonistic roles in the transcriptional feedback oscillator (Claridge-Chang et al., 2001; McDonald and Rosbash, 2001).

Table 3. Mapping metrics for third antennal segment transcriptomes collected after 12 or 48 h of induction of Kir2.1 (K) or a nonconducting control (C)[a]

ID	*n* Reads	*n* Mapped	% Mapped	*n* Unique	% Unique	Average R^2
K12-1	29,660,291	15,855,218	53.46	14,082,433	47.48	0.9939
K12-2	28,904,100	15,808,260	54.69	14,110,730	48.82	0.9943
K12-3	28,938,152	15,549,498	53.73	13,323,889	46.04	0.9935
C12-1	22,023,606	10,963,417	49.78	9,701,601	44.05	0.9941
C12-2	15,850,790	8,864,492	55.93	7,922,966	49.99	0.9947
C12-3	11,834,929	6,237,128	52.70	5,546,857	46.87	0.9946
K48-1	28,004,316	18,815,975	67.19	16,487,747	58.88	0.9953
K48-2	17,661,910	11,229,908	63.58	9,851,297	55.78	0.9951
K48-3	27,158,740	15,643,356	57.60	13,588,111	50.03	0.9957
C48-1	40,636,120	26,365,750	64.88	23,831,661	58.65	0.9770
C48-2	26,993,657	13,344,752	49.44	11,474,648	42.51	0.9612
C48-3	32,525,963	18,944,019	58.24	17,227,196	52.96	0.9787
Average	25,849,381	14,801,814	56.77	13,095,761	50.17	0.9890

[a]Absolute numbers and percentages of reads aligned to Ensembl DM genome release 5.74. *n* Reads, number of raw reads; *n* Mapped and % Mapped, number of reads mapping to the reference genome with corresponding percentage; *n* Unique and % Unique, number of reads mapping to a unique location in the reference genome with corresponding percentage; Average R^2, average replicate correlation (Pearson's correlation coefficient calculated across all genes with a non-zero read count in at least one replicate).

Table 4. Mapping metrics for third antennal segment transcriptomes collected after 96 h of induction of Kir2.1 (K) or a nonconducting control (C)[a]

ID	*n* Reads	*n* Mapped	% Mapped	*n* Unique	% Unique	Average R^2
K96-1	31,213,542	25,030,748	80.19	14,405,148	46.15	0.9836
K96-2	55,190,242	43,522,921	78.86	26,736,203	48.44	0.9937
K96-3	58,556,838	47,205,802	80.62	31,655,311	54.06	0.9941
K96-4	29,803,652	24,632,464	82.65	17,888,586	60.02	0.9933
K96-5	28,647,909	23,564,548	82.26	17,152,909	59.87	0.9937
K96-6	31,030,362	23,420,613	75.48	17,208,103	55.46	0.9925
K96-7	26,014,249	21,066,849	80.98	14,655,033	56.33	0.9932
K96-8	30,622,108	24,934,568	81.43	17,368,348	56.72	0.9928
K96-9	35,563,235	27,845,191	78.30	14,971,400	42.10	0.9869
K96-10	26,388,734	21,106,014	79.98	13,725,816	52.01	0.9904
C96-1	29,748,012	24,036,358	80.80	15,070,224	50.66	0.9928
C96-2	61,127,179	48,487,739	79.32	30,257,167	49.50	0.9933
C96-3	58,864,472	49,116,496	83.44	36,050,234	61.24	0.9939
C96-4	30,582,966	25,278,565	82.66	17,865,165	58.42	0.9928
C96-5	27,223,175	22,593,695	82.99	16,178,509	59.43	0.9935
C96-6	29,951,768	24,706,089	82.49	17,520,016	58.49	0.9908
C96-7	32,514,120	26,933,883	82.84	19,342,591	59.49	0.9940
C96-8	27,902,225	23,365,715	83.74	17,388,108	62.32	0.9936
C96-9	28,058,965	21,639,543	77.12	11,934,889	42.54	0.9911
C96-10	28,737,234	23,114,269	80.43	14,720,484	51.22	0.9928
Average	35,387,049	28,580,104	80.83	19,104,712	54.22	0.9921

[a]Absolute numbers and percentages of reads aligned to Ensembl DM genome release 5.74. *n* Reads, number of raw reads; *n* Mapped and % Mapped, number of reads mapping to the reference genome with corresponding percentage; *n* Unique and % Unique, number of reads mapping to a unique location in the reference genome with corresponding percentage; Average R^2, average replicate correlation (Pearson's correlation coefficient calculated across all genes with a non-zero read count in at least one replicate).

Transcripts encoding olfactory, gustatory, and ionotropic receptors (ORs, GRs, and IRs) provided an index of the purity of our library preparations. Certain ORs, IRs, and GRs are expressed in antennal ORNs but not elsewhere, while others are absent from antennal ORNs but present in different types of sensory neuron (Clyne et al., 1999; Gao and Chess, 1999; Vosshall et al., 1999; Clyne et al., 2000; Dunipace et al., 2001; Scott et al., 2001; Benton et al., 2009). We detected the former, but not the latter, members of all three receptor families, including the obligatory OR coreceptor Orco/Or83b (Larsson et al., 2004), which was expressed at a level above that of all other *OR* genes (mean rLog ± SEM = 13.6178 ± 0.1650), in abundance (Fig. 2*A-C*). These data indicate little, if any, nonantennal contamination of our libraries, and they suggest that receptor gene expression was stable across all experimental conditions.

Table 5. Differentially expressed genes after 12 h of Kir2.1 induction (FDR-adjusted $p < 0.20$)[a]

Gene	Baseline expression	Log_2 fold change	*p*	FDR	Description
CG11550	7106.49	−0.3861	3.07E-06	4.71E-03	lipid binding
Rbfox1	1799.04	0.3151	3.22E-05	1.35E-02	RNA binding
Trc8	885.38	−0.5493	5.29E-05	1.35E-02	protein ubiquitination
baz	2163.42	0.3019	4.58E-05	1.35E-02	cell polarity, junction formation
Dso1	91551.91	−0.2967	4.77E-05	1.35E-02	immune response
lncRNA:noe	89869.98	0.3187	1.95E-05	1.35E-02	no functional information
GstE3	2132.39	0.3211	2.19E-04	4.80E-02	glutathione metabolism
hth	11449.58	0.2245	3.91E-04	6.65E-02	brain development
sff	1232.13	0.4033	3.58E-04	6.65E-02	NMJ development
plum	981.88	0.4713	4.66E-04	7.14E-02	axon pruning
CG11873	977.85	0.3519	6.28E-04	8.74E-02	stress response, transcription
pros	1847.93	0.3498	9.49E-04	1.21E-01	neuronal differentiation
Ank2	4808.04	0.3167	1.68E-03	1.30E-01	membrane scaffolding
CG6421	1256.69	−0.3262	1.70E-03	1.30E-01	immune response
Hcf	801.97	0.5215	1.44E-03	1.30E-01	chromatic remodeling
Kr-h2	805.79	−0.3513	1.59E-03	1.30E-01	membrane organization
Pis	1370.97	0.2670	1.44E-03	1.30E-01	signal transduction
crol	1882.00	0.2505	1.69E-03	1.30E-01	cell adhesion
sdt	1635.14	0.3144	1.52E-03	1.30E-01	cell polarity, junction formation
spz	755.96	0.4628	1.34E-03	1.30E-01	axon guidance, immune response
Syp	3782.12	0.2909	1.84E-03	1.34E-01	RNA binding, NMJ transmission
ATP6AP2	1413.52	−0.3679	2.08E-03	1.45E-01	axonal transport
CG9171	697.10	0.3263	2.27E-03	1.45E-01	O-linked mannosylation
RpL38	9770.50	−0.2603	2.25E-03	1.45E-01	translation
mAcon1	1385.07	−0.3415	2.80E-03	1.65E-01	mitochondrial Krebs cycle
CG3907	2306.39	−0.2459	2.75E-03	1.65E-01	no functional information

[a]*p*, Unadjusted *p* value; FDR, *p* value adjusted for multiple comparisons.

Transcriptomics-friendly manipulation of postsynaptic excitability

Kir2.1, an inwardly rectifying potassium channel, decreases the input resistance of neurons and clamps their membrane potential at or below resting value; it is widely used as a neuronal "silencer" (Johns et al., 1999; Paradis et al., 2001; Burrone et al., 2002). Some single amino acid substitutions in the P-loop signature sequence of the channel (Heginbotham et al., 1994), such as G146S (here called Kir2.1-nc), block ion flow without affecting the protein's localization (Haruna et al., 2007). We generated *Drosophila* codon-optimized *UAS-EGFP::Kir2.1* and *UAS-EGFP::Kir2.1-nc* lines and crossed them to the *GH146-GAL4* driver, which directs transgene expression to PNs (Stocker et al., 1997). Whereas the nonconducting Kir2.1-nc variant proved innocuous, the expression of functional Kir2.1 under *GH146-GAL4* control caused early larval lethality, but this premature death could be circumvented with three tubulin promoter-driven copies of the temperature-sensitive repressor of GAL4, $GAL80^{ts}$ (McGuire et al., 2003), which kept the expression of the channel at bay until the block was thermally relieved during adulthood.

Following their induction for 24 h at 31°C, both EGFP-tagged channels (Kir2.1 and Kir2.1-nc) were detected in PNs of 5-day-old adults at comparable levels and in the same anatomic distribution (Fig. 3*A*). Whole-cell current-clamp recordings showed that EGFP::Kir2.1 lowers the input resistance and membrane time constant relative to EGFP::Kir2.1-nc (Fig. 3*B-D*) and

Table 6. Differentially expressed genes after 48 h of Kir2.1 induction (FDR-adjusted $p < 0.20$)[a]

Gene	Baseline expression	Log_2 fold change	p	FDR	Description
CG8620	36.69	2.2870	1.36E-09	1.27E-05	no functional information
CG42502	7610.35	0.7250	7.72E-07	3.60E-03	no functional information
Hsp27	141.78	1.1780	8.78E-06	2.73E-02	protein folding
BomS3	287.22	1.0470	1.41E-05	3.28E-02	immune response
CR41619	337.93	0.9580	1.77E-05	3.30E-02	no functional information
Fbp2	49.24	−1.3890	3.64E-05	5.65E-02	alcohol dehydrogenase
RpLP2	13612.76	0.7030	4.39E-05	5.84E-02	structural constituent of ribosome
Mst57Dc	10.73	−1.5090	5.61E-05	5.91E-02	mating behavior
S-Lap4	8.45	−1.4820	5.71E-05	5.91E-02	proteolysis
CG5986	566.50	1.0110	6.91E-05	6.44E-02	RNA binding
CG3224	171.53	0.9550	8.83E-05	7.48E-02	ribosomal export
CR31032	31.67	1.4380	1.04E-04	8.06E-02	no functional information
Trx-2	4120.04	0.6480	1.12E-04	8.06E-02	thioredoxin, oxidative stress
Cyp4g1	46.34	−1.5000	1.23E-04	8.23E-02	oxidation-reduction
CG7920	1911.26	−0.6730	1.59E-04	8.23E-02	acetyl CoA metabolism
Hsp67Bc	54.45	1.3110	1.51E-04	8.23E-02	translation, protein folding
Jon65Aiv	22.70	−1.4610	1.52E-04	8.23E-02	proteolysis
mRpS5	722.02	0.7000	1.52E-04	8.23E-02	structural constituent of ribosome
RpS3A	31350.61	0.5610	1.81E-04	8.89E-02	structural constituent of ribosome
Tsp39D	1213.20	0.5520	2.08E-04	9.69E-02	cell membrane scaffolding
CG17454	4301.55	0.5740	3.44E-04	1.50E-01	mRNA splicing
CG6770	41760.18	0.4970	3.70E-04	1.50E-01	transcriptional regulation
Pkd2	10.79	1.3760	3.58E-04	1.50E-01	cation transport
Hsp23	141.98	1.0130	4.67E-04	1.81E-01	protein folding
Obp99d	176.07	1.0220	5.51E-04	1.98E-01	smell perception
snRNA:U2:34ABa	106.57	1.3060	5.49E-04	1.98E-01	mRNA splicing

[a]*p*, Unadjusted *p* value; FDR, *p* value adjusted for multiple comparisons.

Table 7. Differentially expressed genes after 96 h of Kir2.1 induction (FDR-adjusted $p < 0.05$)[a]

Gene	Baseline expression	Log_2 fold change	p	FDR	Description
PGRP-SD	1238.04	−1.6430	3.48E-15	2.70E-11	immune response
Dro	126.09	−2.7530	2.58E-14	1.00E-10	immune response
Hsp26	339.18	1.2540	4.48E-14	1.16E-10	protein folding
pirk	334.11	−1.5010	5.40E-12	1.05E-08	immune response
Obp56a	254.68	−1.1930	9.49E-10	1.48E-06	smell perception
CG10332	160.81	−2.0950	1.48E-09	1.92E-06	no functional information
CG42305	23576.53	1.0490	3.47E-09	3.85E-06	no functional information
Gr32a	76.38	−2.3570	8.22E-09	7.99E-06	smell perception
Hsp23	102.45	1.4180	6.87E-08	5.93E-05	protein folding
ple	2790.60	−0.5390	1.77E-07	1.38E-04	tyrosine hydroxylase
CG42821	879.82	−0.9580	4.02E-07	2.84E-04	no functional information
SiaT	632.96	−0.6810	1.27E-06	8.23E-04	NMJ development
BomS2	73.43	−1.1840	1.73E-06	1.03E-03	immune response
Hsp67Bc	115.73	1.2100	2.45E-06	1.36E-03	translation, protein folding
CG5346	1828.19	−0.5430	3.64E-06	1.89E-03	oxidation/reduction process
Jhe	539.44	−1.6050	8.94E-06	4.35E-03	hormone esterase activity
CG16700	884.33	−0.3650	1.18E-05	5.41E-03	amino acid transporter
CG8303	573.39	−0.7870	1.69E-05	7.29E-03	fatty acyl-CoA metabolism
CG8788	1213.87	0.4020	2.57E-05	9.99E-03	no functional information
Gmap	4141.22	−0.4680	2.44E-05	9.99E-03	vesicle-mediated transport
ZnT63C	451.25	−0.4730	3.00E-05	1.11E-02	zinc transport
Hnf4	1345.62	−0.3230	4.59E-05	1.62E-02	glucose homeostasis
CG12290	3289.24	−0.3730	5.63E-05	1.90E-02	GPCR, rhodopsin-like
BomS1	912.15	−0.7730	9.49E-05	3.07E-02	immune response
CG18302	11179.04	0.3620	1.02E-04	3.15E-02	lipid metabolism
CG3301	759.35	0.4310	1.09E-04	3.15E-02	steroid dehydrogenase
Mmp1	5100.38	−0.3990	1.07E-04	3.15E-02	cell adhesion
AIF	515.32	−0.4530	1.45E-04	3.93E-02	apoptosis inducing factor
CG15890	1533.66	−0.3050	1.46E-04	3.93E-02	transmembrane transporter
BomS3	413.55	−0.7560	1.52E-04	3.94E-02	immune response
Buffy	355.39	0.4910	1.85E-04	4.64E-02	inhibits programmed cell death
CG34456	604.69	0.5120	2.06E-04	5.00E-02	no functional information

[a]*p*, Unadjusted *p* value; FDR, *p* value adjusted for multiple comparisons.

powerfully opposes depolarization: Kir2.1-expressing neurons required approximately twofold larger depolarizing currents to drive spiking across a firing rate range of 1-50 Hz (Fig. 3*E*). Although Kir2.1 does not strictly silence the population of neurons in which it is expressed (the added potassium conductance can always be compensated by a large enough current injection; Fig. 3*B*,*E*), the currents necessary to do so seem difficult to attain *in vivo*.

A simple behavioral test supported this conclusion. Adult-onset expression of Kir2.1 in the PDF-expressing ventral subset of lateral pacemaker neurons (using the *pdf-GAL4* driver) (Renn et al., 1999) disrupted the circadian locomotor rhythm in constant darkness, as expected (Nitabach et al., 2002), whereas flies expressing Kir2.1-nc remained rhythmic (Fig. 3*F*).

Trans-synaptic regulation of gene expression: transmitter release and synapse remodeling, and a late shift to proteostasis and neuroprotection

To delineate changes in presynaptic gene expression after muting postsynaptic neural activity, we compared the third antennal segment transcriptomes of flies expressing either Kir2.1 or Kir2.1-nc in PNs (Fig. 4*A*). We studied three induction times (12, 48, and 96 h) in individuals that were age-matched at the point of analysis: all tissues were harvested between ZT6 and ZT7 on the fifth posteclosion day (Fig. 4*A*). Two sequencing technologies (3′ DGE for the 12 and 48 h groups and standard RNA-seq for the 96 h group) gave similar mapping metrics (Tables 3 and 4).

For 12 h induction, experimental (Kir2.1) and control (Kir2.1-nc) flies were placed at 31°C from ZT18 until ZT6 on their fifth posteclosion day and decapitated between ZT6 and ZT7 on the same day (Fig. 4*A*). Three biological replicates were sequenced for each genotype: one from males and two from females. The inclusion of sex as a variable allowed us to verify that modest expression level changes of low-abundance transcripts could be detected (Shiao et al., 2013). A DESeq2 differential expression analysis based on sex alone returned many known sexually dimorphic ORs at an FDR-adjusted $p < 0.20$, including Or47b (upregulated in males) (Kopp et al., 2008; Shiao et al., 2013), Or85a (upregulated in females) (Kopp et al., 2008), and Or22b (upregulated in females) (Kopp et al., 2008). After sex differences were accounted for and removed by the regression model entered into DESeq2, a comparison of flies expressing Kir2.1 versus Kir2.1-nc in PNs highlighted 25 differentially expressed third antennal segment genes with FDR-adjusted $p < 0.20$ (Table 5). The average changes in absolute expression levels of the top 20 differentially expressed genes were ~15-fold smaller than those of the top 20 clock-controlled genes (log_2 fold changes: 0.35 ± 0.08 for homeostatic genes vs 1.9 ± 0.9 for circadian genes; Tables 2 and 5), resulting in many fewer significant hits for the same FDR threshold. Among genes with the smallest FDR-adjusted *p* values, many are involved in cell fate commitment and morphogenesis (Table 5); eight (*bazooka*, *sugar-free frosting*, *plum*, *prospero*, *Ankyrin 2*, *spätzle*, *Syncrip*, and *ATP6AP2*) have been linked to synaptic organization or synapse

Table 8. Enriched GO biological process terms after 12 h of Kir2.1 induction[a]

GO ID	Term	Annotated	Observed	Expected	Fisher's *p*
GO:0034330	cell junction organization	273	27	14	1.20E-03
GO:0006887	exocytosis	75	11	4	1.80E-03
GO:0016079	synaptic vesicle exocytosis	44	8	2	1.90E-03
GO:0035295	tube development	550	45	29	2.00E-03
GO:0065008	regulation of biological quality	888	66	47	2.20E-03
GO:0060562	epithelial tube morphogenesis	373	33	20	2.40E-03
GO:0007399	nervous system development	843	63	45	2.50E-03
GO:0000209	protein polyubiquitination	58	9	3	3.20E-03
GO:0035239	tube morphogenesis	400	34	21	3.90E-03
GO:0007611	learning or memory	119	14	6	4.00E-03
GO:0050890	cognition	119	14	6	4.00E-03
GO:1901565	organonitrogen compound catabolic process	327	29	17	4.20E-03
GO:0006836	neurotransmitter transport	95	12	5	4.20E-03
GO:0010648	negative regulation of cell communication	241	23	13	4.30E-03
GO:0023057	negative regulation of signaling	241	23	13	4.30E-03
GO:0045055	regulated exocytosis	50	8	3	4.40E-03
GO:0048519	negative regulation of biological process	1047	74	56	4.40E-03
GO:0042391	regulation of membrane potential	51	8	3	5.00E-03
GO:0048729	tissue morphogenesis	483	39	26	5.00E-03
GO:0007610	behavior	377	32	20	5.20E-03
GO:0007269	neurotransmitter secretion	74	10	4	5.40E-03
GO:0099643	signal release from synapse	74	10	4	5.40E-03
GO:0034329	cell junction assembly	176	18	9	5.40E-03
GO:0007613	memory	86	11	5	5.50E-03
GO:0051124	synaptic growth at NMJ	111	13	6	5.70E-03
GO:0007416	synapse assembly	137	15	7	5.80E-03
GO:0007528	neuromuscular junction development	138	15	7	6.20E-03
GO:0060429	epithelium development	730	54	39	6.40E-03
GO:0008582	regulation of synaptic growth at NMJ	88	11	5	6.50E-03
GO:0050808	synapse organization	221	21	12	6.60E-03
GO:0050803	regulation of synapse structure or activity	139	15	7	6.60E-03
GO:0048523	negative regulation of cellular process	914	65	49	6.80E-03
GO:0042752	regulation of circadian rhythm	65	9	3	6.90E-03
GO:0048569	postembryonic animal organ development	371	31	20	7.40E-03
GO:0007267	cell-cell signaling	326	28	17	7.50E-03
GO:0009888	tissue development	786	57	42	7.70E-03
GO:0099003	vesicle-mediated transport in synapse	78	10	4	7.80E-03
GO:0099504	synaptic vesicle cycle	78	10	4	7.80E-03
GO:0010646	regulation of cell communication	595	45	32	8.70E-03
GO:0023051	regulation of signaling	595	45	32	8.70E-03
GO:0007163	establishment or maintenance of cell polarity	171	17	9	9.00E-03
GO:0015672	monovalent inorganic cation transport	92	11	5	9.10E-03
GO:0030163	protein catabolic process	228	21	12	9.30E-03
GO:0002009	morphogenesis of an epithelium	470	37	25	9.30E-03
GO:0006508	proteolysis	471	37	25	9.60E-03
GO:1904396	regulation of NMJ development	93	11	5	9.80E-03
GO:0030100	regulation of endocytosis	46	7	2	1.00E-02

[a]Annotated, number of genes in the universe attached to a GO term; Observed, number of differentially expressed genes (unadjusted $p < 0.05$) attached to a GO term; Expected, number of genes expected by chance to be attached to a GO term.

formation, however indirectly (Doe et al., 1991; Ruiz-Canada et al., 2004; Koch et al., 2008; Pielage et al., 2008; Baas et al., 2011; Sutcliffe et al., 2013; Yu et al., 2013; Halstead et al., 2014; Dubos et al., 2015).

For 48 h induction, experimental and control groups were shifted to 31°C at ZT6 of their third posteclosion day and decapitated between ZT6 and ZT7 on day 5 (Fig. 4*A*). Three biological replicates (all from males) were sequenced for each genotype using 3′ DGE technology. One of the Kir2.1-nc replicates (C48-2) did not cluster well with the others (Table 3) and was excluded from the differential expression analysis, which produced 26 hits with FDR-adjusted $p < 0.20$ (Table 6). Conspicuous among these hits were several ribosomal components and three chaperones of the Hsp20 family (Hsp27, Hsp67Bc, and Hsp23) (Haslbeck et al., 2019). At first glance, the upregulation of heat shock proteins might suggest a direct effect of our method of transgene induction (31°C heat), but on reflection heat cannot explain the observed differences because experimental and control flies were exposed to the same temperature regimen. A more plausible explanation is, therefore, that prolonged postsynaptic silencing places an intense homeostatic burden on presynaptic partners which elicits a generalized increase in protein synthesis.

For 96 h induction, experimental and control groups were kept at 31°C from ZT6 of their first posteclosion day and again decapitated between ZT6 and ZT7 on day 5 (Fig. 4*A*). A total of 20 libraries were sequenced in two batches using RNA-seq technology. A different sequencing method was chosen to ensure that our results were valid across sequencing platforms, and more replicates were processed to increase sensitivity. The first batch consisted of 12 samples with six replicates from each of the two genotypes (all male third antennal segments). Two replicates of each genotype in the first batch (K96-2, K96-3, C96-2, and C96-3) were sequenced to twice the depth of the others to detect very lowly expressed genes more reliably. The second batch (eight samples in total) consisted of another four samples of each genotype: two from females and two from males. Two samples (K96-1 and K96-9) had low within-batch correlations and were omitted from the analysis (Table 4). The increase in statistical power enabled the detection of 32 differentially expressed genes with FDR-adjusted $p < 0.05$ after controlling for sex and batch in DESeq2 (Table 7). Three biological processes stand out among these differentially expressed genes. First, six genes related to the Imd and Toll pathways of the innate immune response (Valanne et al., 2011) were strongly downregulated: the pattern recognition receptor PGRP-SD; the antibacterial peptide Drosocin (Dro); the negative regulator of Imd, pirk; and the antimicrobial peptides Bomanin Short 1, 3, and 5 (also known as IM1, IM2, and IM3). Second, chaperones of the Hsp20 family, already encountered after 48 h induction, were again upregulated (Hsp26, Hsp23, and Hsp67Bc) (Haslbeck et al., 2019). And third, four genes involved in programmed cell death were differentially expressed, with two pro-apoptotic factors downregulated—matrix metalloproteinase 1 (Mmp 1) and apoptosis-inducing factor (AIF)—and two gene products inhibiting apoptosis upregulated (Hsp26, Buffy) (Quinn et al., 2003; H. D. Wang et al., 2004; Joza et al., 2008). Overall, the 96 h picture suggests a transcriptional landscape skewed toward cell protection and maintenance.

To obtain an aerial view of transcriptionally regulated biological processes during all induction periods, we probed for coordinated changes in functionally related sets of genes via GO enrichment analyses. These analyses were performed on all differentially expressed genes with unadjusted $p < 0.05$ and included only GO terms with >40 attached genes; the enriched

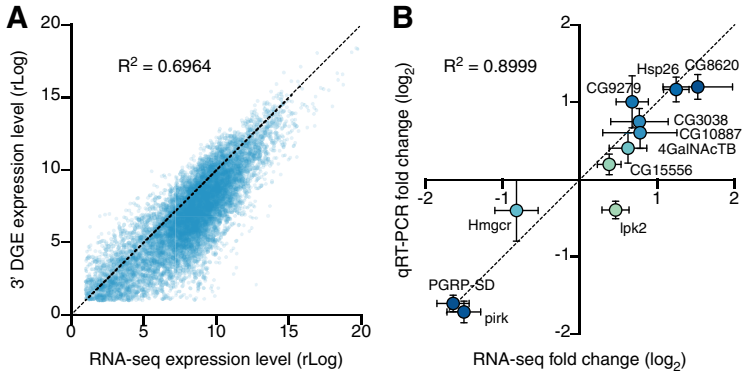

Figure 5. Cross-validation of differential gene expression. ***A***, Scatterplot of average gene expression levels determined by RNA-seq versus 3′ DGE. ***B***, Scatterplot of $\log_2$ fold changes (mean ± SEM) in the expression levels of 11 transcripts after 96 h induction of Kir2.1, determined by RNA-seq or qRT-PCR.

Table 9. Enriched GO biological process terms after 48 h of Kir2.1 induction[a]

GO ID	Term	Annotated	Observed	Expected	Fisher's *p*
GO:0043603	cellular amide metabolic process	405	53	25	8.70E-08
GO:0006518	peptide metabolic process	355	46	22	9.00E-07
GO:0006412	translation	265	37	16	1.90E-06
GO:0043043	peptide biosynthetic process	293	39	18	3.40E-06
GO:0043604	amide biosynthetic process	311	40	19	5.90E-06
GO:0002181	cytoplasmic translation	100	18	6	3.30E-05
GO:0140053	mitochondrial gene expression	86	15	5	2.10E-04
GO:0032543	mitochondrial translation	79	13	5	9.90E-04
GO:1901566	organonitrogen compound biosynthetic process	554	52	34	1.28E-03
GO:0015980	energy derivation by oxidation of organic compounds	54	10	3	1.50E-03

[a]Annotated, number of genes in the universe attached to a GO term; Observed, number of differentially expressed genes (unadjusted $p < 0.05$) attached to a GO term; Expected, number of genes expected by chance to be attached to a GO term.

Table 10. Enriched GO biological process terms after 96 h of Kir2.1 induction[a]

GO ID	Term	Annotated	Observed	Expected	Fisher's *p*
GO:0002181	cytoplasmic translation	100	28	8	5.50E-09
GO:1903825	organic acid transmembrane transport	42	11	4	4.90E-04
GO:1905039	carboxylic acid transmembrane transport	42	11	4	4.90E-04
GO:0043603	cellular amide metabolic process	405	53	34	5.70E-04
GO:0043604	amide biosynthetic process	311	43	26	6.10E-04
GO:0006412	translation	265	38	22	6.30E-04
GO:0006518	peptide metabolic process	355	47	30	9.10E-04
GO:0055114	oxidation-reduction process	308	42	26	9.40E-04
GO:0043043	peptide biosynthetic process	293	40	25	1.22E-03
GO:0009617	response to bacterium	158	25	13	1.32E-03
GO:0015711	organic anion transport	89	16	7	2.59E-03
GO:0046942	carboxylic acid transport	59	12	5	3.03E-03
GO:0015849	organic acid transport	60	12	5	3.51E-03
GO:1901566	organonitrogen compound biosynthetic process	554	63	46	6.21E-03
GO:0034220	ion transmembrane transport	160	23	13	6.94E-03
GO:0098656	anion transmembrane transport	58	11	5	7.74E-03
GO:0006820	anion transport	118	18	10	8.80E-03

[a]Annotated, number of genes in the universe attached to a GO term; Observed, number of differentially expressed genes (unadjusted $p < 0.05$) attached to a GO term; Expected, number of genes expected by chance to be attached to a GO term.

GO terms (Fisher's exact test, $p < 0.01$) were then hierarchically clustered according to their semantic similarity (J. Z. Wang et al., 2007; Brionne et al., 2019) (Fig. 4*B*). After 12 h of induction, presynaptic transcriptional changes centered on genes encoding synaptic release and remodeling machinery; at 48 h and beyond, protein synthesis and degradation, and energy metabolism, predominated (Fig. 4*B*,*C*; Tables 8-10). Closer scrutiny of the 81 genes responsible for the early enrichment of synaptic GO annotations (Fig. 4*C*; Tables 11 and 12) uncovered many with established roles in homeostatic plasticity at the NMJ (or with known interactions with such genes), as we discuss below. Although typical transcripts showed only modest expression level changes of 15%-30%, their regulation was clearly visible across multiple libraries (Fig. 4*C*). This consistency across biological replicates, and the statistically verified overabundance of synaptic genes in the differentially expressed set with low unadjusted *p* values (Tables 11 and 12), suggest a genuine signal.

Cross-validation of regulated genes with 3′ DGE, RNA-seq, and qRT-PCR

As a further validation of our gene expression measurements, we compared transcriptome-wide 3′ DGE with transcriptome-wide RNA-seq data. There was an approximately linear relationship between the average expression levels of all genes in all samples (Fig. 5*A*), with a small departure in lowly expressed genes caused by the extra amplification step in the RNA-seq protocol (see Materials and Methods); as a result, RNA-seq reported systematically higher expression levels for scarce transcripts than did 3′ DGE. For genes transcribed at moderate to high expression levels, the two sequencing platforms were in close agreement.

We next selected 11 transcripts for qRT-PCR verification. These transcripts were chosen from the set of differentially expressed genes (unadjusted $p < 0.05$; both upregulated and downregulated) in the 96 h induction group and used to validate all deep sequencing data. The fold changes of the 11 chosen transcripts, as estimated by qRT-PCR with normalization to the housekeeping gene *CycK*, correlated tightly with 3′ DGE and RNA-seq measurements (Fig. 5*B*). This agreement between three independent measures of gene expression, at a transcriptome-wide scale and across several individual genes, lends confidence to our analysis.

Discussion

Trans-synaptic regulation of gene expression

Our study introduces an experimental system for detecting changes in gene expression in response to changes in the electrical excitability of a partner cell. The product of the *Kir2.1* transgene powerfully suppresses the activity of neurons in which it is expressed, while a control transgene, which codes for a potassium channel with a single amino acid substitution in its selectivity filter, has no effect (Fig. 3*B-F*). Isogenic strains expressing one or the other of these transgenes from the same chromosomal locus offer an ideal platform for differential gene expression analyses because differences between them can be pinned to a single codon change in the genome. The finding that prolonged postsynaptic silencing induces the expression of Hsp20 proteins in a

Table 11. Differentially expressed genes ($p < 0.05$) attached to GO biological process terms in the semantic grouping "transmitter release" after 12 h of Kir2.1 induction

Gene	Baseline expression	Log_2 fold change	*p*
Ank2	4808.04	0.3167	1.68E-03
crol	1882.00	0.2505	1.69E-03
Syp	3782.12	0.2909	1.84E-03
ATP6AP2	1413.52	−0.3679	2.08E-03
Pngl	165.57	−0.5711	2.84E-03
Nsf2	57.11	1.0758	4.99E-03
sky	574.22	0.4143	5.49E-03
CG13796	98.20	0.7603	5.64E-03
rab3-GEF	74.57	0.9719	5.81E-03
Atpalpha	25649.53	0.2121	7.80E-03
rept	43.03	−0.9271	1.06E-02
nSyb	7467.28	0.1791	1.25E-02
Cirl	753.00	0.2911	1.37E-02
Teh1	490.53	0.3833	1.47E-02
CG17278	103.00	−0.6499	1.91E-02
Grd	36.96	−0.9307	1.93E-02
Cby	442.89	−0.3202	2.13E-02
Syx6	229.68	−0.4827	2.22E-02
rl	129.67	0.5579	2.28E-02
Vha100-2	1861.65	−0.2887	2.39E-02
eag	1418.20	0.2192	2.62E-02
NAAT1	301.63	−0.3582	2.92E-02
qvr	751.52	0.2494	2.93E-02
Rab5	6457.41	0.1526	3.09E-02
kto	125.71	0.5835	3.33E-02
Csp	246.20	−0.3718	3.50E-02
Rdl	9593.74	0.1719	3.67E-02
para	15702.82	0.1020	3.70E-02
CASK	2105.66	0.1889	3.73E-02
stmA	1105.17	−0.2661	4.04E-02
Hk	1229.40	0.1803	4.22E-02
disp	51.74	−0.7734	4.23E-02
nonC	55.67	0.7504	4.33E-02
unc-13-4A	244.53	0.3676	4.53E-02
Wnk	233.48	0.4181	4.57E-02
cpx	9807.02	0.1367	4.78E-02
sgg	3797.38	0.1451	4.83E-02
CG31030	278.71	0.3348	4.92E-02
dor	43.31	−0.7143	4.99E-02

Table 12. Differentially expressed genes ($p < 0.05$) attached to GO biological process terms in the semantic grouping "synapse remodeling" after 12 h of Kir2.1 induction

Gene	Baseline expression	Log_2 fold change	*p*
Rbfox1	1799.04	0.3151	3.22E-05
baz	2163.42	0.3019	4.58E-05
sff	1232.13	0.4033	3.58E-04
plum	981.88	0.4713	4.66E-04
Piezo	200.21	−0.6974	6.79E-04
pros	1847.93	0.3498	9.49E-04
spz	755.96	0.4628	1.34E-03
sdt	1635.14	0.3144	1.52E-03
ken	135.28	0.6630	2.10E-03
Su(dx)	557.27	−0.4424	4.47E-03
krz	352.41	0.4352	4.47E-03
awd	1639.43	−0.3123	4.61E-03
Patr-1	38.20	1.0956	6.97E-03
HDAC4	3937.61	0.1914	7.18E-03
alph	1833.82	0.3419	8.46E-03
jus	1553.93	−0.2206	1.04E-02
Khc-73	1436.43	0.2236	1.07E-02
CG14806	119.88	0.6016	1.07E-02
Syn1	224.74	0.4885	1.60E-02
Med	127.02	−0.6286	1.66E-02
pck	104.18	−0.6858	1.71E-02
Ulp1	140.50	0.6389	1.91E-02
Ote	25.41	1.0066	1.92E-02
vsg	1464.00	−0.2474	1.94E-02
hop	663.22	−0.1699	2.02E-02
Nup75	250.20	0.3893	2.12E-02
scrib	1348.95	−0.2035	2.65E-02
Adar	479.31	0.3031	2.78E-02
ci	133.51	−0.5603	2.86E-02
Ect4	958.87	0.2181	2.95E-02
hiw	264.24	0.3638	3.48E-02
RhoGAP54D	9.86	1.1083	3.48E-02
Gprk2	635.86	0.3247	3.50E-02
Ube3a	161.07	−0.4591	3.51E-02
Nak	219.26	−0.4719	3.60E-02
CG10188	43.14	−0.9196	4.28E-02
CG18659	166.96	−0.4214	4.41E-02
fmt	983.41	0.2500	4.52E-02
Mmp1	3792.36	0.2127	4.57E-02
CG5521	26.02	0.9428	4.65E-02
ex	55.44	0.7311	4.73E-02
CrebB	1128.36	0.2159	4.86E-02
EloB	691.48	−0.2662	4.99E-02

manner unrelated to heat shock (Tables 6 and 7) underscores the power of this carefully controlled system.

The same finding, however, also highlights a limitation particular to our current approach. We imposed the Kir2.1 clamp on the first synaptic relay in the *Drosophila* olfactory system because its presynaptic and postsynaptic elements are easily separable by purely physical means, but this convenience exacted a price: the third antennal segment contains not only ORNs but also glial and support cells, which account for approximately two-thirds of the segment's cell population (Vosshall et al., 1999). We are therefore unable to determine whether the expression of Hsp20 proteins is exclusively or even partially neuronal. Although the same reservation does not apply to the many synaptic genes that are differentially expressed during the early phase of the homeostatic response (Fig. 4*B*,*C*), the presence of non-neuronal elements may nevertheless have hindered the detection of low-abundance neuronal transcripts or underestimated their fold change. Both of these drawbacks could be overcome by FACS isolation of a genetically labeled cell population from dissociated neural tissue, as would be required as a matter of course in all instances where the synaptic partners are intermingled. With this extra step (which we were unable to take because antennal tissue could not be recovered intact from its chitinous shell), our system will be easily adapted for analyses of transcriptional changes elicited in presynaptic cells by a loss of postsynaptic responsivity, in postsynaptic cells by a loss of presynaptic input, or in glial cells by a heightened demand for synaptic remodeling.

Despite these caveats, many of the early expression level changes we detect affect genes encoding synaptic proteins with known, suspected, or at least plausible roles in homeostatic plasticity (Fig. 4*B*,*C*; Tables 5, 11, and 12) (Davis and Müller, 2015): elements of the wingless signaling system (e.g., Wnk, sgg), which acts as an endogenous suppressor of homeostatic compensation at the NMJ (Marie et al., 2010); the v-SNARE synaptobrevin (nSyb) and its chaperone Nsf2 (Söllner et al., 1993; Bacci et al., 2001); rab3 guanine nucleotide exchange factor (rab3-GEF), which controls the assembly and distribution of active zone

components (Bae et al., 2016) and regulates the nucleotide state-dependent association of rab3 with synaptic vesicles, which in turn determines the calcium sensitivity of their release (Geppert et al., 1997; Müller et al., 2011); an active zone resident (unc-13-4a) known to associate with the Rab3-interacting molecule RIM and other active zone components (Schoch et al., 2002; Liu et al., 2011; Müller et al., 2012); a kinesin motor heavy chain (Khc-73) implicated in active zone assembly and synaptic homeostasis (Tsurudome et al., 2010); an active zone-integral guanylate kinase (CASK) that serves as a phosphorylation target of CDK5 (Samuels et al., 2007), which homeostatically regulates presynaptic calcium influx and release probability (Seeburg et al., 2008; S. H. Kim and Ryan, 2010); the E3 ubiquitin-protein ligase highwire (hiw) and the Smad protein Medea (Med), which in motor neuron terminals are part of the transduction cascade for a retrograde signal from muscle (Haghighi et al., 2003; McCabe et al., 2004; Goold and Davis, 2007); the cytoskeletal anchor Ankyrin 2 (Koch et al., 2008; Pielage et al., 2008); and subunits or accessory proteins of voltage-gated ion channels (quiver, ether-á-go-go, Hyperkinetic, paralytic) (Tables 5, 11, and 12). Collectively, these changes could signal an increase in the number of release sites or an expansion of the release-ready vesicle pool, inferred to represent the dominant quantal parameter change during homeostatic matching at ORN-to-PN synapses (Kazama and Wilson, 2008) and one of two homeostatic levers at the NMJ (the other being modulation of calcium influx into the terminal) (Müller et al., 2012).

When drawing comparisons with earlier work, however, it is important to bear in mind differences in the speed of induction and expression of the homeostatic response. Abrupt adult-onset PN silencing resembles an acute postsynaptic receptor blockade at the NMJ more closely than it does the slow developmental processes studied in analyses of arbor size matching in the antennal lobe (Kazama and Wilson, 2008; Mosca and Luo, 2014), but homeostatic compensation at the NMJ is evident within minutes, long before changes in gene expression can occur (Frank et al., 2006). That elements of the homeostatic machinery are encoded by trans-synaptically regulated genes must therefore reflect a secondary layer of feedback or the more profound reallocation of ORN synapses between PNs and other postsynaptic partners, such as local neurons of the antennal lobe (Groschner and Miesenböck, 2019).

Because changes in the expression levels of putative homeostatic genes are small compared with those of circadian-regulated genes (Figs. 1*D*, 4*C*), we were forced to relax our FDR thresholds in the 12 and 48 h induction experiments, raising the specter of false positives in these datasets. Two observations should allay this concern. First, the 96 h induction experiment, whose greater statistical power allowed a more stringent significance threshold, recovered many of the same biological processes and indeed the same genes (e.g., Hsp23, Hsp67Bc) as the statistically weaker 48 h induction experiment (Tables 9 and 10). Second, our qRT-PCR validation included several genes that failed to cross the most stringent FDR threshold (Fig. 5*B*). These qRT-PCR spot checks confirmed that expression level changes detected by RNA-seq or 3′ DGE were accurate. Nonetheless, new candidates emerging from our screen will need to survive rigorous functional studies before joining the ranks of established homeostatic plasticity genes.

Labeling connections with trans-synaptically regulated genes?

In many neurobiological studies, the object of interest is not a population of genetically homogeneous neurons but an operational unit (a circuit) defined by connectivity rather than a common genetic marker. Circuit analyses have benefited greatly from the development of trans-synaptic vectors, which travel along synaptic connections between specific types of neuron and serve as vehicles for the distribution of other encodable tools (Miesenböck and Kevrekidis, 2005; Miesenböck, 2009; Sjulson et al., 2016). Ideally, trans-synaptic expression systems possess a mechanism that allows their initialization at a specific location, a rule that governs their propagation in the network, and gain. Viruses have some of these characteristics (Strack et al., 1989; Ugolini et al., 1989; Card et al., 1990; Wickersham et al., 2007). Their infectious spread can follow routes of synaptic transmission, and replicative gain (where permitted) allows each infected neuron to supply more viral particles to its outputs than it receives from its inputs. Viral infections are, however, difficult to control and initialize with single-cell resolution and can produce considerable toxicity and extrasynaptic spread. Clearly, the ideal trans-synaptic vector would, instead of carrying its own genetic material, act on expression cassettes that lie dormant in the genome of the host organism until switched on by a trans-synaptic signal.

Circuit-tracing systems such as *trans*-Tango, TRACT, and BAcTrace are built on this principle but require the reconstitution of an exogenous cell-to-cell signaling apparatus (Huang et al., 2017; Talay et al., 2017; Cachero et al., 2020). This adds genetic complexity and the danger of overexpression artifacts if the foreign molecules escape synaptic confinement. Eavesdropping on endogenous trans-synaptic communication during homeostatic plasticity offers a possible cure for these problems. Imagine a sudden, targeted loss of excitability in a small group of neurons or even a single cell, brought about by the inducible expression of Kir2.1. If presynaptic partners compensate for this perturbation, the upregulation of plasticity genes could be coupled to the expression of sensors, actuators, transcription factors, or recombinases.

The chief obstacle to the development of this retrograde tracing technology is the small, at most twofold, changes in homeostatic gene expression we detect (Tables 5, 11, and 12). We suspect that these changes will need to be amplified with adequate signal-to-noise ratio, perhaps by flipping a recombination switch, to be practically useful. The application of this strategy to immediate early genes serves as an encouraging precedent: immediate early genes are used widely to trap neural ensembles in defined functional contexts, although their activity-dependent expression level changes roughly equal those of our trans-synaptically regulated genes (Sjulson et al., 2016; DeNardo and Luo, 2017). And while the degree or direction of homeostatic adjustment may vary among synapses (Turrigiano, 2011), the substantial overlap between elements of the homeostatic machinery at the NMJ (Davis and Müller, 2015) and homeostatically regulated genes in the antennal lobe (Fig. 4*C*) points to a conserved mechanistic core.

References

Alexa A, Rahnenführer J, Lengauer T (2006) Improved scoring of functional groups from gene expression data by decorrelating GO graph structure. Bioinformatics 22:1600–1607.

Andrews S (2010) FastQC: a quality control tool for high throughput sequence data. https://www.bioinformatics.babraham.ac.uk/projects/fastqc/.

Baas S, Sharrow M, Kotu V, Middleton M, Nguyen K, Flanagan-Steet H, Aoki K, Tiemeyer M (2011) Sugar-free frosting, a homolog of SAD

kinase, drives neural-specific glycan expression in the *Drosophila* embryo. Development 138:553–563.

Bacci A, Coco S, Pravettoni E, Schenk U, Armano S, Frassoni C, Verderio C, De Camilli P, Matteoli M (2001) Chronic blockade of glutamate receptors enhances presynaptic release and downregulates the interaction between synaptophysin-synaptobrevin-vesicle-associated membrane protein 2. J Neurosci 21:6588–6596.

Bae H, Chen S, Roche Diagnostics JP, Ai M, Wu C, Diantonio A, Graf ER (2016) Rab3-GEF controls active zone development at the *Drosophila* neuromuscular junction. eNeuro 3:ENEURO.0031-16.2016.

Benton R, Vannice KS, Gomez-Diaz C, Vosshall LB (2009) Variant ionotropic glutamate receptors as chemosensory receptors in *Drosophila*. Cell 136:149–162.

Bolger AM, Lohse M, Usadel B (2014) Trimmomatic: a flexible trimmer for Illumina sequence data. Bioinformatics 30:2114–2120.

Brionne A, Juanchich A, Hennequet-Antier C (2019) ViSEAGO: a Bioconductor package for clustering biological functions using Gene Ontology and semantic similarity. BioData Min 12:16.

Burrone J, O'Byrne M, Murthy VN (2002) Multiple forms of synaptic plasticity triggered by selective suppression of activity in individual neurons. Nature 420:414–418.

Cachero S, Gkantia M, Bates AS, Frechter S, Blackie L, McCarthy A, Sutcliffe B, Strano A, Aso Y, Jefferis GS (2020) BAcTrace, a tool for retrograde tracing of neuronal circuits in *Drosophila*. Nat Methods 17:1254–1261.

Card JP, Rinaman L, Schwaber JS, Miselis RR, Whealy ME, Robbins AK, Enquist LW (1990) Neurotropic properties of pseudorabies virus: uptake and transneuronal passage in the rat central nervous system. J Neurosci 10:1974–1994.

Claridge-Chang A, Wijnen H, Naef F, Boothroyd C, Rajewsky N, Young MW (2001) Circadian regulation of gene expression systems in the *Drosophila* head. Neuron 32:657–671.

Clyne PJ, Warr CG, Carlson JR (2000) Candidate taste receptors in *Drosophila*. Science 287:1830–1834.

Clyne PJ, Warr CG, Freeman MR, Lessing D, Kim J, Carlson JR (1999) A novel family of divergent seven-transmembrane proteins: candidate odorant receptors in *Drosophila*. Neuron 22:327–338.

Cull-Candy SG, Miledi R, Trautmann A, Uchitel OD (1980) On the release of transmitter at normal, myasthenia gravis and myasthenic syndrome affected human end-plates. J Physiol 299:621–638.

Davis GW, DiAntonio A, Petersen SA, Goodman CS (1998) Postsynaptic PKA controls quantal size and reveals a retrograde signal that regulates presynaptic transmitter release in *Drosophila*. Neuron 20:305–315.

Davis GW, Müller M (2015) Homeostatic control of presynaptic neurotransmitter release. Annu Rev Physiol 77:251–270.

DeNardo L, Luo L (2017) Genetic strategies to access activated neurons. Curr Opin Neurobiol 45:121–129.

Desai NS, Rutherford LC, Turrigiano GG (1999) Plasticity in the intrinsic excitability of cortical pyramidal neurons. Nat Neurosci 2:515–520.

Doe CQ, Chu-LaGraff Q, Wright DM, Scott MP (1991) The prospero gene specifies cell fates in the *Drosophila* central nervous system. Cell 65:451–464.

Donlea JM, Pimentel D, Miesenböck G (2014) Neuronal machinery of sleep homeostasis in *Drosophila*. Neuron 81:860–872.

Dubos A, Castells-Nobau A, Meziane H, Oortveld MA, Houbaert X, Iacono G, Martin C, Mittelhaeuser C, Lalanne V, Kramer JM, Bhukel A, Quentin C, Slabbert J, Verstreken P, Sigrist SJ, Messaddeq N, Birling MC, Selloum M, Stunnenberg HG, Humeau Y, et al. (2015) Conditional depletion of intellectual disability and Parkinsonism candidate gene ATP6AP2 in fly and mouse induces cognitive impairment and neurodegeneration. Hum Mol Genet 24:6736–6755.

Dunipace L, Meister S, McNealy C, Amrein H (2001) Spatially restricted expression of candidate taste receptors in the *Drosophila* gustatory system. Curr Biol 11:822–835.

Frank CA, Kennedy MJ, Goold CP, Marek KW, Davis GW (2006) Mechanisms underlying the rapid induction and sustained expression of synaptic homeostasis. Neuron 52:663–677.

Gao Q, Chess A (1999) Identification of candidate *Drosophila* olfactory receptors from genomic DNA sequence. Genomics 60:31–39.

Geppert M, Goda Y, Stevens CF, Südhof TC (1997) The small GTP-binding protein Rab3A regulates a late step in synaptic vesicle fusion. Nature 387:810–814.

Goold CP, Davis GW (2007) The BMP ligand Gbb gates the expression of synaptic homeostasis independent of synaptic growth control. Neuron 56:109–123.

Goold CP, Nicoll RA (2010) Single-cell optogenetic excitation drives homeostatic synaptic depression. Neuron 68:512–528.

Groschner LN, Miesenböck G (2019) Mechanisms of sensory discrimination: insights from *Drosophila* olfaction. Annu Rev Biophys 48:209–229.

Haghighi AP, McCabe BD, Fetter RD, Palmer JE, Hom S, Goodman CS (2003) Retrograde control of synaptic transmission by postsynaptic CaMKII at the *Drosophila* neuromuscular junction. Neuron 39:255–267.

Halstead JM, Lin YQ, Durraine L, Hamilton RS, Ball G, Neely GG, Bellen HJ, Davis I (2014) Syncrip/hnRNP Q influences synaptic transmission and regulates BMP signaling at the *Drosophila* neuromuscular synapse. Biol Open 3:839–849.

Haruna Y, Kobori A, Makiyama T, Yoshida H, Akao M, Doi T, Tsuji K, Ono S, Nishio Y, Shimizu W, Inoue T, Murakami T, Tsuboi N, Yamanouchi H, Ushinohama H, Nakamura Y, Yoshinaga M, Horigome H, Aizawa Y, Kita T, et al. (2007) Genotype-phenotype correlations of KCNJ2 mutations in Japanese patients with Andersen-Tawil syndrome. Hum Mutat 28:208.

Haslbeck M, Weinkauf S, Buchner J (2019) Small heat shock proteins: simplicity meets complexity. J Biol Chem 294:2121–2132.

Heginbotham L, Lu Z, Abramson T, MacKinnon R (1994) Mutations in the K^+ channel signature sequence. Biophys J 66:1061–1067.

Huang TH, Niesman P, Arasu D, Lee D, De La Cruz AL, Callejas A, Hong EJ, Lois C (2017) Tracing neuronal circuits in transgenic animals by transneuronal control of transcription (TRACT). Elife 6:e32027.

Johns DC, Marx R, Mains RE, O'Rourke B, Marbán E (1999) Inducible genetic suppression of neuronal excitability. J Neurosci 19:1691–1697.

Joza N, Galindo K, Pospisilik JA, Benit P, Rangachari M, Kanitz EE, Nakashima Y, Neely GG, Rustin P, Abrams JM, Kroemer G, Penninger JM (2008) The molecular archaeology of a mitochondrial death effector: AIF in *Drosophila*. Cell Death Differ 15:1009–1018.

Kazama H, Wilson RI (2008) Homeostatic matching and nonlinear amplification at identified central synapses. Neuron 58:401–413.

Kim D, Pertea G, Trapnell C, Pimentel H, Kelley R, Salzberg SL (2013) TopHat2: accurate alignment of transcriptomes in the presence of insertions, deletions and gene fusions. Genome Biol 14:R36.

Kim SH, Ryan TA (2010) CDK5 serves as a major control point in neurotransmitter release. Neuron 67:797–809.

Koch I, Schwarz H, Beuchle D, Goellner B, Langegger M, Aberle H (2008) *Drosophila* Ankyrin 2 is required for synaptic stability. Neuron 58:210–222.

Kopp A, Barmina O, Hamilton AM, Higgins L, McIntyre LM, Jones CD (2008) Evolution of gene expression in the *Drosophila* olfactory system. Mol Biol Evol 25:1081–1092.

Larsson MC, Domingos AI, Jones WD, Chiappe ME, Amrein H, Vosshall LB (2004) Or83b encodes a broadly expressed odorant receptor essential for *Drosophila* olfaction. Neuron 43:703–714.

Liu KS, Siebert M, Mertel S, Knoche E, Wegener S, Wichmann C, Matkovic T, Muhammad K, Depner H, Mettke C, Bückers J, Hell SW, Müller M, Davis GW, Schmitz D, Sigrist SJ (2011) RIM-binding protein, a central part of the active zone, is essential for neurotransmitter release. Science 334:1565–1569.

Livak KJ, Schmittgen TD (2001) Analysis of relative gene expression data using real-time quantitative PCR and the $2^{-\Delta\Delta CT}$ method. Methods 25:402–408.

Love MI, Huber W, Anders S (2014) Moderated estimation of fold change and dispersion for RNA-seq data with DESeq2. Genome Biol 15:550.

Marie B, Pym E, Bergquist S, Davis GW (2010) Synaptic homeostasis is consolidated by the cell fate gene gooseberry, a *Drosophila* pax3/7 homolog. J Neurosci 30:8071–8082.

McCabe BD, Hom S, Aberle H, Fetter RD, Marques G, Haerry TE, Wan H, O'Connor MB, Goodman CS, Haghighi AP (2004) Highwire regulates presynaptic BMP signaling essential for synaptic growth. Neuron 41:891–905.

McDonald MJ, Rosbash M (2001) Microarray analysis and organization of circadian gene expression in *Drosophila*. Cell 107:567–578.

McGuire SE, Le PT, Osborn AJ, Matsumoto K, Davis RL (2003) Spatiotemporal rescue of memory dysfunction in *Drosophila*. Science 302:1765–1768.

Miesenböck G (2009) The optogenetic catechism. Science 326:395–399.

Miesenböck G, Kevrekidis IG (2005) Optical imaging and control of genetically designated neurons in functioning circuits. Annu Rev Neurosci 28:533–563.

Mosca TJ, Luo L (2014) Synaptic organization of the *Drosophila* antennal lobe and its regulation by the Teneurins. eLife 3:e03726.

Müller M, Pym EC, Tong A, Davis GW (2011) Rab3-GAP controls the progression of synaptic homeostasis at a late stage of vesicle release. Neuron 69:749–762.

Müller M, Liu KS, Sigrist SJ, Davis GW (2012) RIM controls homeostatic plasticity through modulation of the readily-releasable vesicle pool. J Neurosci 32:16574–16585.

Nitabach MN, Blau J, Holmes TC (2002) Electrical silencing of *Drosophila* pacemaker neurons stops the free-running circadian clock. Cell 109:485–495.

Paradis S, Sweeney ST, Davis GW (2001) Homeostatic control of presynaptic release is triggered by postsynaptic membrane depolarization. Neuron 30:737–749.

Petersen SA, Fetter RD, Noordermeer JN, Goodman CS, DiAntonio A (1997) Genetic analysis of glutamate receptors in *Drosophila* reveals a retrograde signal regulating presynaptic transmitter release. Neuron 19:1237–1248.

Pfeiffer BD, Ngo TT, Hibbard KL, Murphy C, Jenett A, Truman JW, Rubin GM (2010) Refinement of tools for targeted gene expression in *Drosophila*. Genetics 186:735–755.

Pielage J, Cheng L, Fetter RD, Carlton PM, Sedat JW, Davis GW (2008) A presynaptic giant ankyrin stabilizes the NMJ through regulation of presynaptic microtubules and transsynaptic cell adhesion. Neuron 58:195–209.

Quinn L, Coombe M, Mills K, Daish T, Colussi P, Kumar S, Richardson H (2003) Buffy, a *Drosophila* Bcl-2 protein, has anti-apoptotic and cell cycle inhibitory functions. EMBO J 22:3568–3579.

Renn SC, Park JH, Rosbash M, Hall JC, Taghert PH (1999) A pdf neuropeptide gene mutation and ablation of PDF neurons each cause severe abnormalities of behavioral circadian rhythms in *Drosophila*. Cell 99:791–802.

Ruiz-Canada C, Ashley J, Moeckel-Cole S, Drier E, Yin J, Budnik V (2004) New synaptic bouton formation is disrupted by misregulation of microtubule stability in aPKC mutants. Neuron 42:567–580.

Samuels BA, Hsueh YP, Shu T, Liang H, Tseng HC, Hong CJ, Su SC, Volker J, Neve RL, Yue DT, Tsai LH (2007) Cdk5 promotes synaptogenesis by regulating the subcellular distribution of the MAGUK family member CASK. Neuron 56:823–837.

Sandrock AW, Dryer SE, Rosen KM, Gozani SN, Kramer R, Theill LE, Fischbach GD (1997) Maintenance of acetylcholine receptor number by neuregulins at the neuromuscular junction in vivo. Science 276:599–603.

Schoch S, Castillo PE, Jo T, Mukherjee K, Geppert M, Wang Y, Schmitz F, Malenka RC, Südhof TC (2002) RIM1alpha forms a protein scaffold for regulating neurotransmitter release at the active zone. Nature 415:321–326.

Scott K, Brady R, Cravchik A, Morozov P, Rzhetsky A, Zuker C, Axel R (2001) A chemosensory gene family encoding candidate gustatory and olfactory receptors in *Drosophila*. Cell 104:661–673.

Seeburg DP, Feliu-Mojer M, Gaiottino J, Pak DT, Sheng M (2008) Critical role of CDK5 and Polo-like kinase 2 in homeostatic synaptic plasticity during elevated activity. Neuron 58:571–583.

Shiao MS, Fan WL, Fang S, Lu MY, Kondo R, Li WH (2013) Transcriptional profiling of adult *Drosophila* antennae by high-throughput sequencing. Zool Stud 52:42.

Sjulson L, Cassataro D, DasGupta S, Miesenböck G (2016) Cell-specific targeting of genetically encoded tools for neuroscience. Annu Rev Genet 50:571–594.

Söllner T, Whiteheart SW, Brunner M, Erdjument-Bromage H, Geromanos S, Tempst P, Rothman JE (1993) SNAP receptors implicated in vesicle targeting and fusion. Nature 362:318–324.

Stocker RF, Heimbeck G, Gendre N, de Belle JS (1997) Neuroblast ablation in *Drosophila* P[GAL4] lines reveals origins of olfactory interneurons. J Neurobiol 32:443–456.

Strack AM, Sawyer WB, Hughes JH, Platt KB, Loewy AD (1989) A general pattern of CNS innervation of the sympathetic outflow demonstrated by transneuronal pseudorabies viral infections. Brain Res 491:156–162.

Sutcliffe B, Forero MG, Zhu B, Robinson IM, Hidalgo A (2013) Neuron-type specific functions of DNT1, DNT2 and Spz at the *Drosophila* neuromuscular junction. PLoS ONE 8:e75902.

Talay M, Richman EB, Snell NJ, Hartmann GG, Fisher JD, Sorkaç A, Santoyo JF, Chou-Freed C, Nair N, Johnson M, Szymanski JR, Barnea G (2017) Transsynaptic mapping of second-order taste neurons in flies by trans-Tango. Neuron 96:783–795.e4.

Thiagarajan TC, Lindskog M, Tsien RW (2005) Adaptation to synaptic inactivity in hippocampal neurons. Neuron 47:725–737.

Trapnell C, Roberts A, Goff L, Pertea G, Kim D, Kelley DR, Pimentel H, Salzberg SL, Rinn JL, Pachter L (2012) Differential gene and transcript expression analysis of RNA-seq experiments with TopHat and Cufflinks. Nat Protoc 7:562–578.

Tsurudome K, Tsang K, Liao EH, Ball R, Penney J, Yang JS, Elazzouzi F, He T, Chishti A, Lnenicka G, Lai EC, Haghighi AP (2010) The *Drosophila* miR-310 cluster negatively regulates synaptic strength at the neuromuscular junction. Neuron 68:879–893.

Turrigiano G (2011) Too many cooks? Intrinsic and synaptic homeostatic mechanisms in cortical circuit refinement. Annu Rev Neurosci 34:89–103.

Turrigiano G, Abbott LF, Marder E (1994) Activity-dependent changes in the intrinsic properties of cultured neurons. Science 264:974–977.

Turrigiano GG, Leslie KR, Desai NS, Rutherford LC, Nelson SB (1998) Activity-dependent scaling of quantal amplitude in neocortical neurons. Nature 391:892–896.

Ugolini G, Kuypers HG, Strick PL (1989) Transneuronal transfer of herpes virus from peripheral nerves to cortex and brainstem. Science 243:89–91.

Valanne S, Wang JH, Rämet M (2011) The *Drosophila* Toll signaling pathway. J Immunol 186:649–656.

Vosshall LB, Amrein H, Morozov PS, Rzhetsky A, Axel R (1999) A spatial map of olfactory receptor expression in the *Drosophila* antenna. Cell 96:725–736.

Wang HD, Kazemi-Esfarjani P, Benzer S (2004) Multiple-stress analysis for isolation of *Drosophila* longevity genes. Proc Natl Acad Sci USA 101:12610–12615.

Wang JZ, Du Z, Payattakool R, Yu PS, Chen CF (2007) A new method to measure the semantic similarity of GO terms. Bioinformatics 23:1274–1281.

Wickersham IR, Lyon DC, Barnard RJ, Mori T, Finke S, Conzelmann KK, Young JA, Callaway EM (2007) Monosynaptic restriction of transsynaptic tracing from single, genetically targeted neurons. Neuron 53:639–647.

Wierenga CJ, Ibata K, Turrigiano GG (2005) Postsynaptic expression of homeostatic plasticity at neocortical synapses. J Neurosci 25:2895–2905.

Yu XM, Gutman I, Mosca TJ, Iram T, Ozkan E, Garcia KC, Luo L, Schuldiner O (2013) Plum, an immunoglobulin superfamily protein, regulates axon pruning by facilitating TGF-β signaling. Neuron 78:456–468.